Proliferation and Differentiation of Transplantable Rabbit Epithelial Sheets Engineered with or without an Amniotic Membrane Carrier

Kazunari Higa,[1] *Shigeto Shimmura,*[1,2] *Naoko Kato,*[2] *Tetsuya Kawakita,*[1] *Hideyuki Miyashita,*[2] *Yuji Itabashi,*[3] *Keiichi Fukuda,*[3] *Jun Shimazaki,*[1,2] *and Kazuo Tsubota*[1,2]

Purpose. To report a novel method of engineering transplantable, carrier-free corneal epithelial sheets by using a biodegradable fibrin sealant and to compare its characteristics with epithelial sheets cultivated on denuded amniotic membrane carriers.

Methods. Stratified corneal epithelial sheets were prepared in culture dishes coated with biodegradable fibrin glue. Amniotic membrane (AM) carriers served as the control. The quality of cultivated sheets was compared by immunohistochemistry for cytokeratin (K)3, K12, K14, p63, occludin, and integrin β1; electron microscopy; and colony-forming assays. K3 protein expression was compared by Western blot analysis. In a limbal-deficient rabbit transplantation model, postoperative adaptation and proliferation of BrdU-labeled cell sheets were examined by histology and anti-Ki67 staining.

Results. Epithelial sheets were successfully engineered by using a biodegradable fibrin sealant. Cell sheets in both groups were multilayered, expressed K3, K12, and K14, and had functioning occludin$^+$ apical tight junctions as well as p63 and integrin β1 staining in basal cells. The carrier-free sheets appeared to be more differentiated than the AM sheets, which was also demonstrated by the higher levels of K3 in the Western blots. The colony-forming efficiency of dissociated cells was similar in both groups, although larger colonies were observed on the AM sheets. AM sheets retained higher levels of BrdU-labeled cells and fewer Ki67$^+$ cells compared with carrier-free sheets after transplantation.

Conclusions. Tissue engineering with a commercially available fibrin sealant was an effective means of creating a carrier-free, transplantable corneal epithelial sheet. Carrier-free sheets were more differentiated compared with AM sheets, while retaining similar levels of colony-forming progenitor cells. (*Invest Ophthalmol Vis Sci.* 2007;48:597-604) DOI:10.1167/iovs.06-0664

From the [1]Department of Ophthalmology, Tokyo Dental College, Chiba, Japan; and the Departments of [2]Ophthalmology and [3]Regenerative Medicine and Advanced Cardiac Therapeutics, Keio University School of Medicine, Tokyo, Japan.

Supported in part by a grant from Advanced and Innovational Research Program in Life Sciences from the Ministry of Education, Culture, Sports, Science and Technology (TK) and a Grant-in-Aid for Scientific Research (SS).

Submitted for publication June 15, 2006; revised September 22, 2006; accepted December 14, 2006.

Disclosure: **K. Higa**, None; **S. Shimmura**, None; **N. Kato**, None; **T. Kawakita**, None; **H. Miyashita**, None; **Y. Itabashi**, None; **K. Fukuda**, None; **J. Shimazaki**, None; **K. Tsubota**, None

The publication costs of this article were defrayed in part by page charge payment. This article must therefore be marked "*advertisement*" in accordance with 18 U.S.C. §1734 solely to indicate this fact.

Corresponding author: Shigeto Shimmura, Department of Ophthalmology, Keio University School of Medicine, 35 Shinanomachi, Shinjuku-ku, Tokyo 160-8582, Japan; shige@sc.itc.keio.ac.jp.

Investigative Ophthalmology & Visual Science, February 2007, Vol. 48, No. 2

The use of allogenic or autologous cell sources for regenerative surgery is already common practice in the reconstruction of the ocular surface in patients with stem cell deficiency.[1,2] After the success of limbal transplantation, a second generation of regenerative corneal surgery has emerged in the form of cell sheet transplantation by tissue-engineering techniques.[3] Cell sheet transplants currently in clinical use are prepared by using biological carriers such as fibrin[4] or amniotic membrane (AM)[5-7] or as carrier-free cell sheets.[8,9] Although there is still debate as to whether the cultivated sheets include progenitor or stem cells, both carrier and carrier-free techniques have restored a clear ocular surface for at least 1 year, the empiric goal for successful stem cell surgery.[7,9]

One of the major benefits of cell sheet transplants, is that it can avoid the problem of donor availability. In vitro expansion provides a stratified cell sheet suitable for transplantation from a millimeter-scale tissue source procured from the healthy eye of the same patient or from a living relative in the case of bilateral disease. Ectopic cell sources such as the buccal membrane can also be modified in vitro to form a stratified epithelial sheet for ocular surface reconstruction with autologous tissue.[9-11] Yet, the number of clinical cases has not met the needs of patients because of ethical and technical constraints. Using AM as a carrier is one possibility as a standardized technique to produce transplantable epithelial sheets; however, AM tissue may not be readily available.

The development of a carrier-free method to produce corneal epithelial sheets was first reported by Nishida et al.,[8] who used a novel temperature-responsive polymer that changes molecular conformation and hydrophobicity at 20°C to release intact sheets. Clinical cases in which this technique has been used have shown that a carrier-free strategy is feasible and that transplantation can be performed without the use of sutures. In the present study, we developed a different technique by using commercially available fibrin sealants to produce carrier-free sheets. Our method is different from the fibrin carrier sheets described by Rama et al.,[4] as we allowed the fibrin to be degraded by intrinsic proteases before transplantation.

Materials and Methods

Antibodies

Mouse monoclonal antibodies (mAbs) for cytokeratin (K)3, K14, laminin, p63, integrin β1, and Ki67 were purchased from Progen (AE5; Heidelberg, German), Abcam (B429; Cambridgeshire, UK), Laboratory Vision (4C7; Fremont, CA), Calbiochem (4A4; Merck KGaA, Darmstadt, Germany), Chemicon International Inc. (LM534; Temecula, CA), and DakoCytomation (MIB-1; Glostrup, Denmark), respectively. Mouse IgM antibody for fibrin was purchased from Monosan (Uden, The Netherlands). Rabbit polyclonal antibody for K12, goat polyclonal antibody for type IV collagen and rat mAb for BrdU (ICR1) were purchased from TransGenic, Inc. (Kumamoto, Japan), Southern Biotechnology Associates, Inc. (Birmingham, AL) and Abcam. Isotype goat IgG, mouse IgG1,

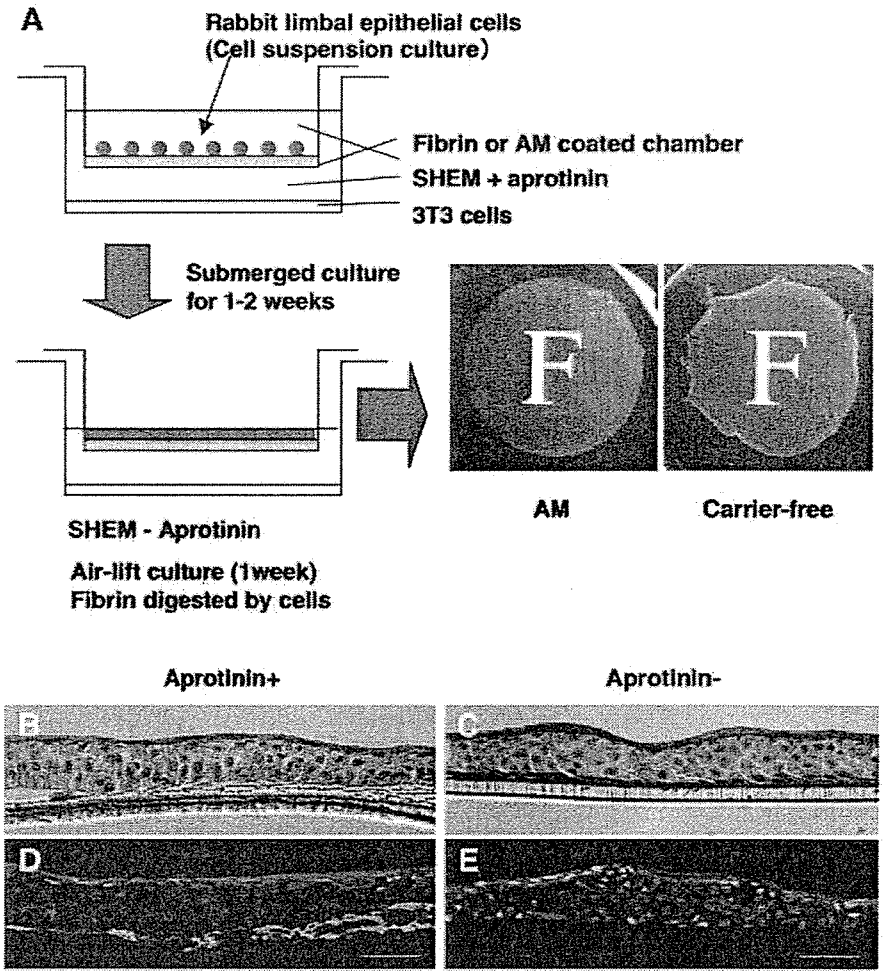

FIGURE 1. Cultivation of carrier-free epithelial sheets. Limbal epithelial cells were collected and seeded on fibrin- or AM-coated chambers (A). After 1 to 2 weeks in submerged culture with MMC-treated 3T3 feeder fibroblasts, the cells were allowed to stratify at the air–liquid interface for 1 week. HE staining (B, C) and immunohistochemistry against fibrin (*green*) and K12 (*red*) (D, E) showed that fibrin acted as a scaffold during cultivation with the protease inhibitor aprotinin (B, D) and was allowed to dissolve by removing the aprotinin before transplantation (C, E).

mouse IgM, rabbit IgG and rat IgG as control were purchased from Santa Cruz Biotechnology (Santa Cruz, CA), Dako Cytomation, and Jackson ImmunoResearch Laboratories (West Grove, PA), respectively. FITC-, rhodamine-, and Cy3-conjugated secondary antibodies were purchased from Jackson ImmunoResearch Laboratories and Chemicon International Inc.

Preparation of Epithelial Cells Sheets

All experimental procedures and protocols were approved by the Animal Care and Use Committee of Tokyo Dental College and conformed to the National Instituted of Health Guide for the Care and Use of Laboratory Animals. Fibrin sealant was purchased from Fujisawa (Bolheal; Osaka, Japan), and its constitution was performed as reported previously.[12] In brief, a solution containing 40 mg of human fibrinogen and 0.18 U of thrombin was diluted with 7.5 mL saline, and 0.3 mL was spread rapidly onto the upper chambers of a six-well plate with culture inserts (Transwell; Costar Corning, Corning, NY). Two hours later, the polymerized fibrin-coated top chambers were obtained and stored at 4°C. AMs were donated by mothers who were seronegative for human immunodeficiency virus and hepatitis B and C virus at the time of cesarean section, after written informed consent was obtained, in accordance with the Declaration of Helsinki. AM was stored with 15% dimethylsulfoxide (Sigma-Aldrich, St. Louis, MO) with PBS at −80°C until use. Denuded AM was prepared as previously described.[7] Membranes were rinsed in PBS, spread onto the upper chambers of a six-well insert, frozen at −80°C, and air-dried at room temperature.

Primary cultures of limbal epithelial cells were prepared from eyes of 2.5- to 3.0-kg female Japanese white rabbits (Japan CLEA, Tokyo, Japan) with anesthesia induced by intravenous injection of 4 mL pentobarbital sodium (50 mg/mL). Limbal rims of corneoscleral tissue were prepared by careful removal of excess sclera, iris, corneal endothelium, and central cornea. Epithelial sheets were isolated as described previously.[13] Dispersed epithelial sheets were treated with trypsin-ethylenediaminetetracetic acid (EDTA) for 10 minutes, to suspend cells, which were seeded onto fibrin- or AM-coated wells (2×10^5 cells/mL) with supplemented hormonal epithelial medium (SHEM)[7] containing 666 KIU/mL aprotinin (Wako, Osaka, Japan) and cocultured with mitomycin C (MMC)-treated 3T3 fibroblasts (Fig. 1A). The cultures were submerged in medium until confluence, cultured in air–liquid interface for 1 week, and finally incubated without aprotinin for 4 days. To evaluate the proliferation of transplanted epithelium and to identify cells of donor origin, cell sheets were labeled with 10 μM BrdU for 48 hours before surgery. After labeling with BrdU, the epithelial cell sheets were washed with fresh medium and then used for surgery.

Transmission Electron Microscopy

Epithelial cell sheets were processed for transmission electron microscopy. Epithelial cell sheets from both groups were fixed in 2.5% glutaraldehyde solution in 60 mM HEPES buffer solution for 4 hours. After washing, samples were postfixed in 1% osmium tetroxide, dehydrated in a series of ethanol and propylene oxide, and embedded in epoxy resin. Semithin sections (1-μm) were stained with toluidine blue. Then, ultrathin specimens were sectioned with a microtome (LKB, Gaithersburg, MD). Sections in the range of gray to silver were collected on 150-mesh grid, stained with uranyl acetate and lead

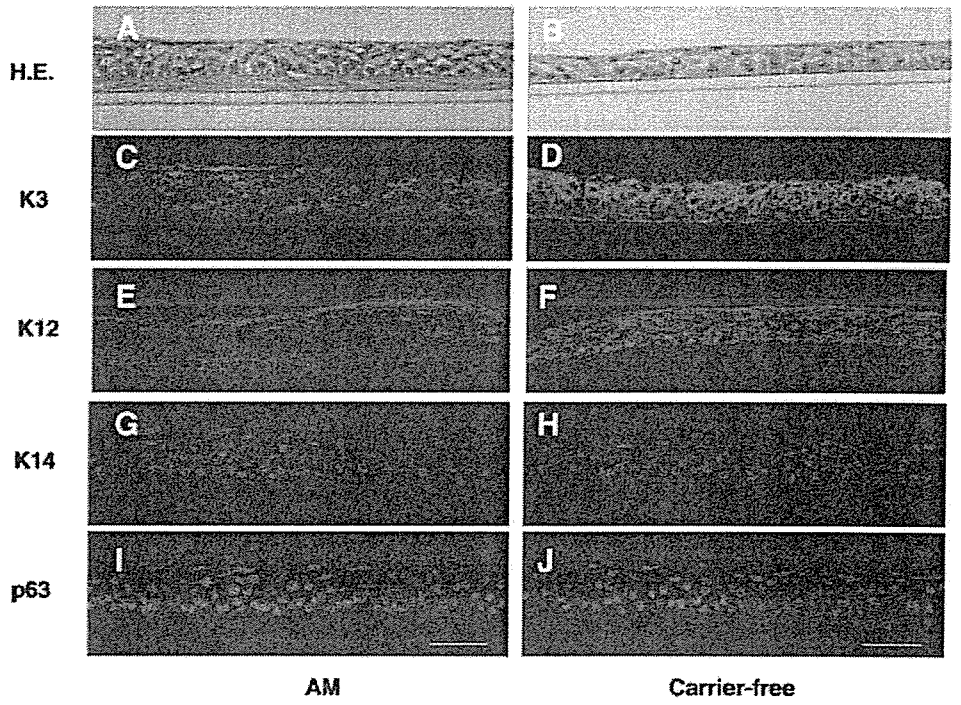

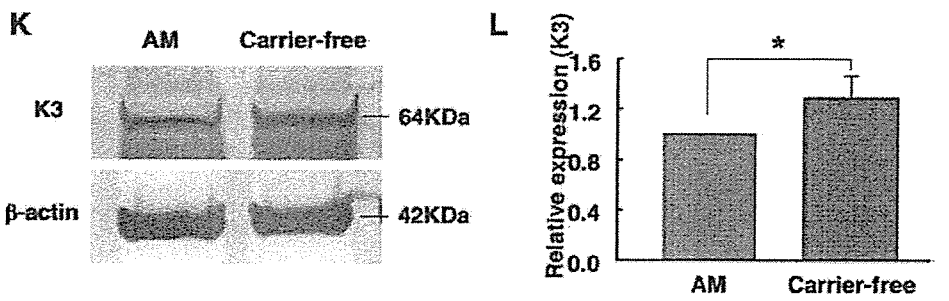

FIGURE 2. Differentiation markers in epithelial sheets. Hematoxylin and eosin staining of AM (A) and carrier-free (B) epithelial cell sheets. (C–J) Immunohistochemistry of K3, K12, K14, and p63 in epithelial sheets. Carrier-free sheets showed stronger K3/K12 staining and weaker K14/p63 staining than did AM sheets. Nuclei of cells were stained with DAPI. Scale bar, 50 μm. The difference in K3 expression was confirmed by Western blot (K), which showed significantly higher levels of K3 in carrier-free sheets than in AM sheets, when compared semiquantitatively (L, $n = 6$, $^*P = 0.002$).

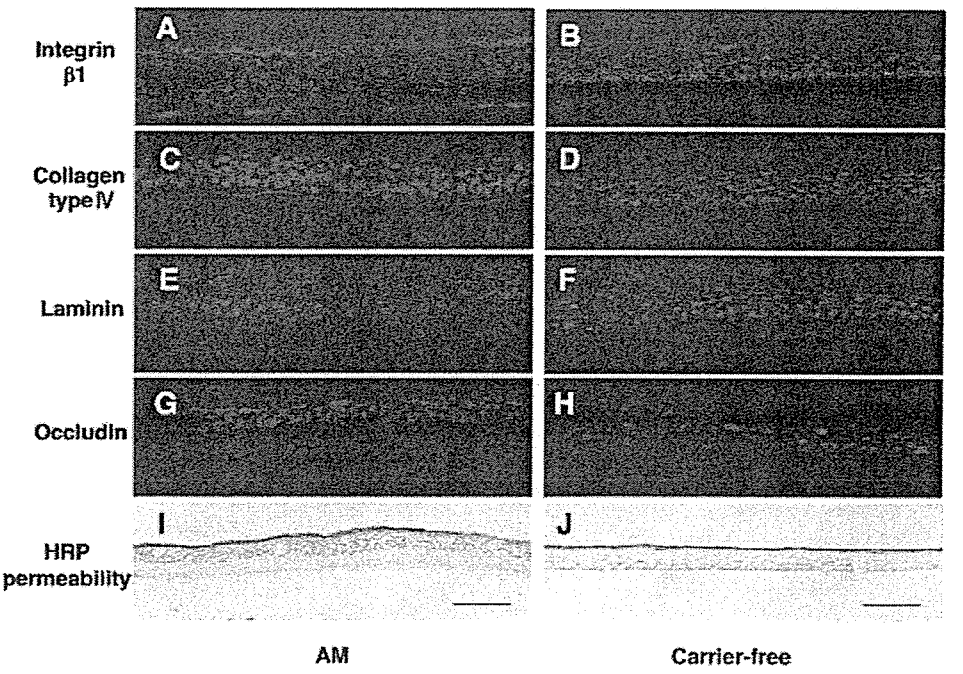

FIGURE 3. Basement membrane components and barrier function in epithelial sheets. Immunohistochemistry of integrin β1, collagen type IV, laminin, and occludin in AM (A, C, E, G) and carrier-free (B, D, F, H) epithelial sheets. Nuclei of cells were stained with DAPI. (I, J) Barrier function (HRP permeability) of the epithelial sheets. Scale bar, 50 μm.

citrate, and examined under an electron microscope (model 1200 EXII; JEOL, Tokyo, Japan).

Colony-Forming Efficiency

To evaluate the proliferative potential of cells in the cultured sheets, MMC-treated 3T3 fibroblasts were used in a colony-forming efficiency (CFE) assay, as previously described.[14–16] NIH 3T3 fibroblasts in DMEM containing 10% FCS were treated with MMC (4 μg/mL) for 2 hours at 37°C and then treated with trypsin-EDTA and plated at a density of 3×10^6 cells in 100-mm culture dishes. Single cells were prepared from both treated epithelial cell sheets (Acutase; Innovative Cell Technologies, Inc., San Diego, CA) for 60 minutes at 37°C. Each dish was seeded at 1×10^3 cells/dish. CFE was calculated by the percentage of colonies at day 14 generated by the number of epithelial cells plated in the dish. Quantification of size (in square millimeters) and number of colonies obtained from AM or fibrin sheets ($n = 5$) was performed by NIH Image (available by ftp at zippy.nimh.nih.gov/ or at http://rsb.info.nih.gov/nih-image; developed by Wayne Rasband, National Institutes of Health, Bethesda, MD). Growth capacity was evaluated on day 14 when cultured cells were stained with rhodamine B (Wako) for 30 minutes.

Epithelial Sheet Transplantation

All animals were handled in full accordance with the ARVO Statement for the Use of Animals in Ophthalmic and Vision Research and institutional guidelines. Rabbits were anesthetized with intramuscular injection of xylazine hydrochloride (2.5 mg/mL) and ketamine hydrochloride (37.5 mg/mL). The left eye in each rabbit was rendered totally limbal stem cell deficient by 1-*n*-heptanol (Sigma-Aldrich) mechanical debridement of the corneal epithelium, and surgical removal of the limbal and conjunctival epithelium was performed up to 2 mm from the limbus. Carrier-free sheets were gently detached from the mesh with a cell scraper,[12] transferred by microforceps and then expanded on the bare corneal stroma with a surgical sponge or forceps. Cell sheets were allowed to attach for 5 minutes without sutures. AM carrier sheets were sutured to the corneal surface with 10-0 nylon sutures. Rabbits with denuded corneas without sheet transplants served as the control. After surgery, all rabbits were fitted with a bandage contact lens and topical antibiotic (levofloxacin), and steroids (betamethasone) were applied twice daily.

The percentage of the cornea covered by epithelium at 1 week after surgery was calculated by measuring the area of the epithelial defects. The defect area was analyzed by tracing fluorescein images and calculated using the NIH Image program. Rabbits were then killed to observe BrdU-labeled cells as a means to confirm the donor origin of epithelium. The proliferation of transplanted epithelial cells was examined by calculating the percentage of $BrdU^+$ and $Ki67^+$ nuclei by immunohistochemistry.

Immunohistochemistry

Paraffin sections (K3, K14, p63, BrdU, and Ki67) were deparaffinized in xylene and rehydrated. Frozen sections (type IV collagen and laminin) were fixed for 10 minutes in cold acetone before blocking. Frozen sections (integrin β1 and K12) were fixed for 10 minutes in 2% paraformaldehyde (Wako). Sections were blocked by incubation with 10% normal donkey serum (Chemicon International Inc., Temecula, CA) and 1% bovine serum albumin (Sigma-Aldrich) for 1 hour at room temperature (RT). Antibodies to K3 (1:50), K12 (1:100), K14 (1:100), p63 (1:50), BrdU (1:100), Ki67 (1:50), type IV collagen (1:50), laminin (1:50), and integrin β1 (1:100) were applied and incubated for 90 minutes at RT, followed by incubation with rhodamine- or Cy3-conjugated secondary antibody. After three washes with TBST, the sections were incubated with 1 mg/mL 4′,6-diamidino-2-phenylindole (DAPI; Dojindo Laboratories, Tokyo, Japan) at RT for 5 minutes. Finally, the sections were washed three times in TBST and coverslipped after mounting with an antifade medium (50 mM Tris buffer saline, 90% glycerin; Wako), 10% 1,4-diazabicyclo-2,2,2-octane (Wako).

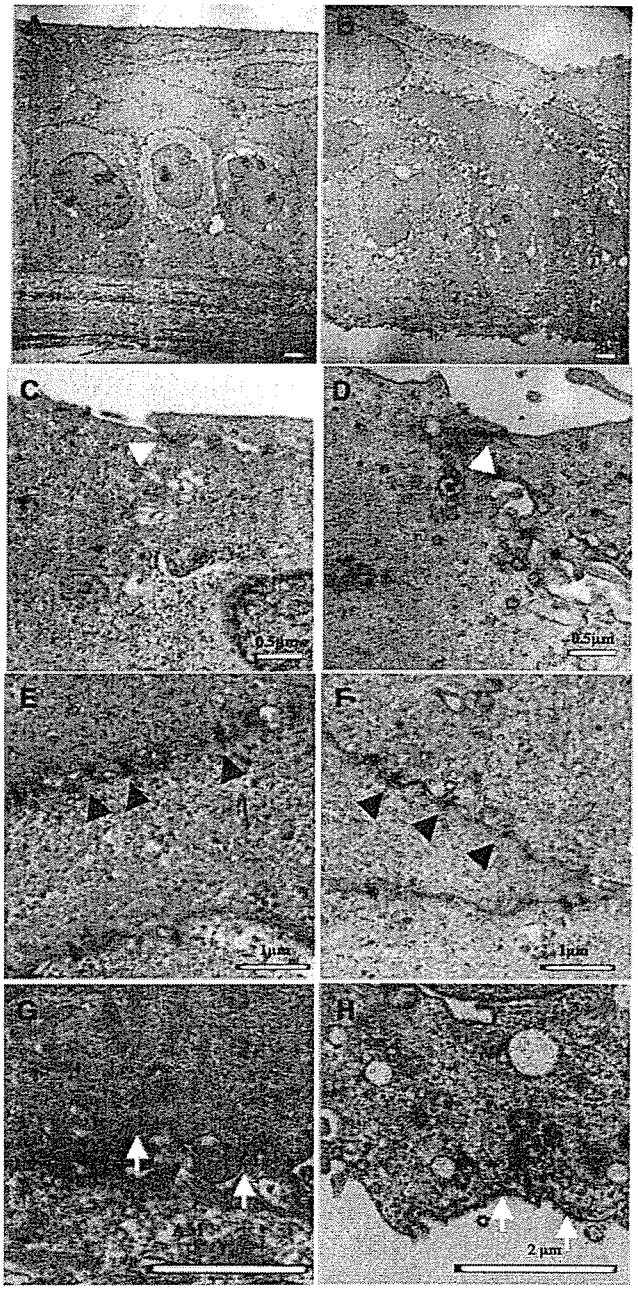

FIGURE 4. Transmission electron micrographs of AM and carrier-free sheets. Both AM (**A**, **C**, **E**, **G**) and carrier-free (**B**, **D**, **F**, **H**) sheets formed five to six layers of well-stratified epithelial cells, with columnar basal epithelial cells. High-magnification views show tight junction formation in apical cells (**C**, **D**, *white arrowheads*), and desmosome formation in the intermediate layers (**E**, **F**, *black arrowheads*). Basal cells formed an intact basement membrane in the AM sheets (**G**, *arrows*), whereas carrier-free sheets had residual material attached to the basal cell membrane (**H**, *white arrows*).

Western Blot Analysis

Epithelial sheets were dissociated with lysis buffer (50 mM Tris-HCl [pH 7.4], 150 mM NaCl, 1% Nonidet P-40; Calbiochem, Darmstadt, Germany) and homogenized. Each epithelial cell sheet was incubated for 40 minutes at 4°C, and then centrifuged at 15,000 rpm for 30 minutes at 4°C. Protein concentration of the supernatant was deter-

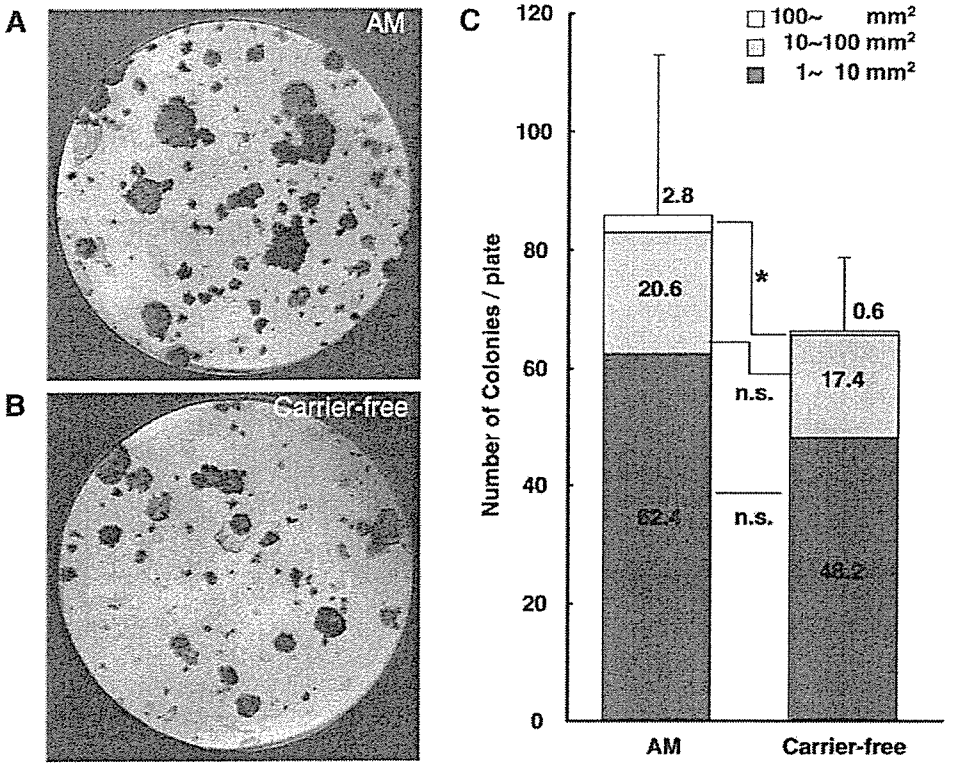

FIGURE 5. Colony formation by disassembled cells. Colony formation by epithelial cells dissociated from AM (A) and carrier-free (B) sheets. Colonies were stained with rhodamine B after 2 weeks. (C) Quantification of size and number of colonies obtained from epithelial sheets (n = 5, mean ± SD). There was no significant difference in total colony formation. When cultures were compared by the area of each colony, a significant difference was observed only in the largest colony size (*P = 0.014; Student's t-test, n = 5).

mined by a protein assay (DC assay; Bio-Rad Laboratory, Hercules, CA). All samples were then diluted in 2× sample buffer (100 mM Tris-HCl [pH 6.8]), 4% SDS (Invitrogen, Carlsbad, CA), 20% glycerol (Wako), 12% 2-mercaptoethanol (Wako), and boiled. Ten micrograms of each sample were loaded on a 10% Bis-Tris gel (Novex NuPAGE; Invitrogen) and transferred onto polyvinylidene difluoride (PVDF) membranes (Millipore, Billerica, MA). The membranes were blocked with 5% skim milk (Difco Laboratories, Detroit, MI), 1.5% normal goat serum, and PBS for 60 minutes at RT. The membranes were reacted with K3 (AE5) and β-actin (mabcam8226; Abcam) for 60 minutes at RT. After the membranes were washed three times in TBST, donkey biotinylated anti-mouse IgG (Jackson ImmunoResearch Laboratories) was added for 30 minutes at room temperature. Protein bands were visualized (Vectastain ABC Elite Kit; Vector Laboratories, Burlingame, CA) with DAB (Vector Laboratories) as the substrate. The plot profile of the bands was analyzed with the NIH image 1.63 software with band density of AM sheets in each group standardized at 1.0.

Statistical Analysis

Statistical comparisons of Western blot band intensity, CFE, epithelialization, and BrdU and Ki67 staining were performed with the nonpaired Student's t-test (Excel; Microsoft, Redmond, WA).

RESULTS

Generation of Carrier-Free Epithelial Cell Sheets

Rabbit corneal epithelial cells were cultured with 3T3 feeder cells for 1 to 2 weeks, followed by airlift cultures to produce stratified epithelium on plastic coated with fibrin polymer (Fig. 1A). Fibrin remained at the bottom of the cell sheet when cultured with aprotinin (Figs. 1B, 1D) and was dissolved after removal of aprotinin, presumably due to intrinsic proteolytic activity (Figs. 1C, 1E).

In Vitro Characteristics of Cultivated Sheets

We performed a comparative study of carrier-free corneal epithelial sheets with epithelial sheet cultivated on AM carriers. Stratified epithelium was engineered on both AM (Fig. 2A) and plastic coated with degradable fibrin polymer (Fig. 2B). The use of aprotinin did not affect cell growth or stratification on the AM carriers.

Immunohistochemistry using anti-K3 and K12 antibodies showed that carrier-free cultures produced uniform layers of cells expressing both differentiation markers (Figs. 2C–F). Sporadic cells in the basal layer were K3 negative, which is characteristic of immature limbal basal cells in vivo. Both AM and carrier-free sheets expressed K14 (Figs. 2G, 2H) and p63 (Figs. 2I, 2J). The epithelium on AM carriers appeared to express higher levels of K14 and p63, and less K3, K12, suggesting that the AM maintains epithelial cells in a less differentiated state. The difference in K3 expression was also demonstrated by Western blot analysis (Figs. 2K, 2L). Both AM and carrier-free sheets show an intact superficial tight junction, as shown by immunohistochemistry of occludin (Figs. 3G, 3H) and the exclusion of HRP (Figs. 3I, 3J). Basement membrane components such as collagen IV and laminin were more prominent in the AM sheet in vitro (Figs. 3C, 3E). These proteins were not as evident in the carrier-free sheets before transplantation (Figs. 3D, 3F). However, the adhesion molecule integrin β1 was expressed in both sheets (Figs. 3A, 3B).

Transmission electron microscopy revealed that the ultrastructure of the epithelium was similar between the AM and carrier-free sheets, consisting of five to six layers of stratified epithelial cells with typical columnar basal cells and superficial cells with microvilli (Figs. 4A, 4B). Both cells sheets showed tight junction formation in apical cells (Figs. 4C, 4D) and desmosome formation (Figs. 4E, 4F). Although a basement membrane structure was observed in AM sheets (Fig. 4G), the carrier-free sheets showed residual material attached to the

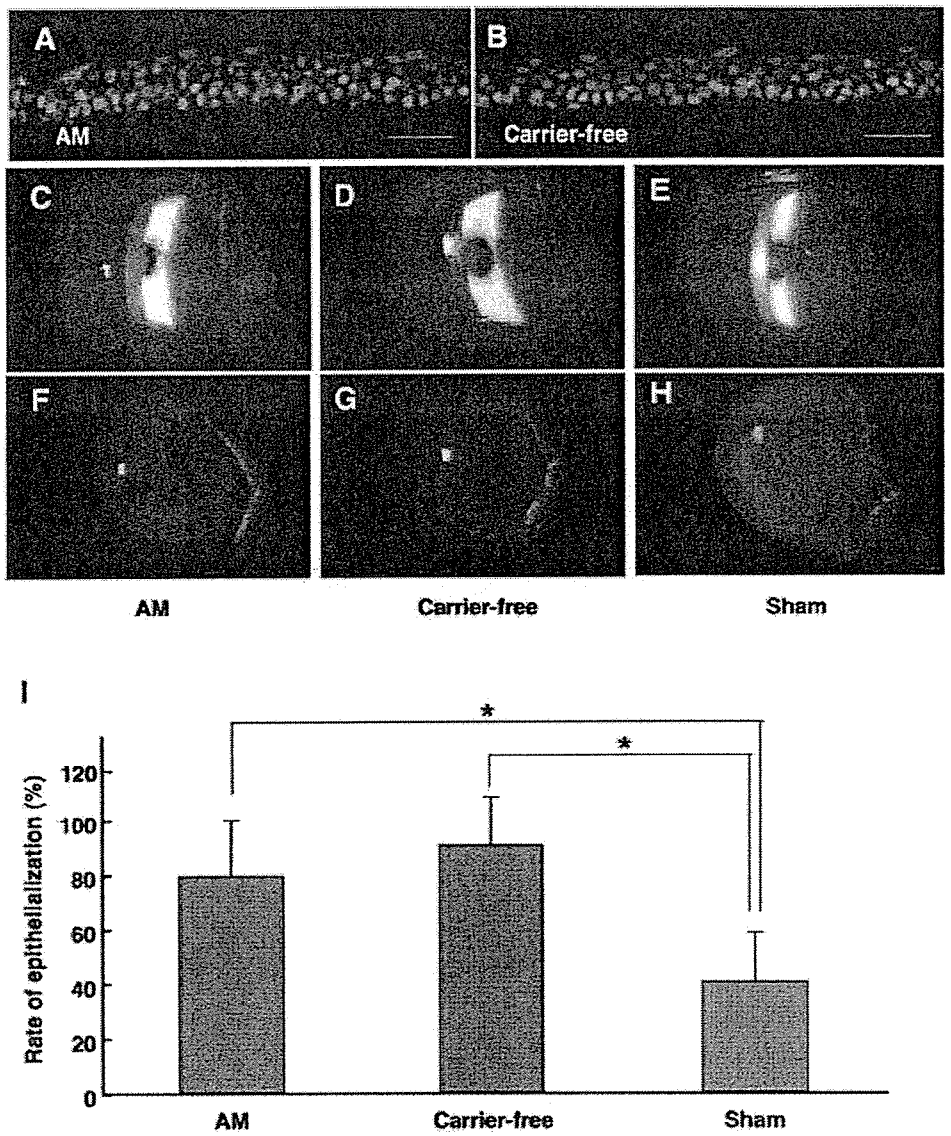

FIGURE 6. Epithelial sheet transplantation in rabbits. Immunohistochemistry of BrdU (A, B) in epithelial sheets before transplantation. Slit lamp photographs (C–E) and fluorescein staining (F–H) of rabbit eyes 1 week after epithelial sheet transplantation. (C, F) AM, (D, G) carrier-free, (E, H) sham. (I) Area of intact epithelium was larger in rabbit eyes after epithelial sheet transplantation compared with sham ($^*P < 0.05$). Carrier-free sheets had a smoother epithelial surface with minimal inflammation. Scale bar, 50 μm.

basal epithelial membrane (Fig. 4H) which may represent components of the basement membrane structure such as integrin β1, collagen IV, and laminin observed by immunohistochemistry (Figs. 3B, 3D, 3F).

Colony-Forming Efficiency

Isolated epithelial cells from both carrier-free (6.6% ± 1.2%) and AM carrier sheets (8.6% ± 2.7%) maintained the ability to form colonies in a 3T3 feeder layer (Figs. 5A, 5B). Although the number of large colonies (100 mm^2) was higher in AM sheets (AM: 2.8 ± 1.3 colonies, fibrin: 0.6 ± 0.8 colonies, $P = 0.014$, $n = 5$), the difference in the total number of colonies was not statistically significant (Fig. 5C).

Cultivated Sheet Transplantation

BrdU labeling was performed on the AM (Fig. 6A) and carrier-free (Fig. 6B) sheets before surgery, showing that most of the cells in both groups are viable with proliferative potential. Rabbits without cell sheet transplants characteristically had epithelial defects at 1 week after surgery, as shown by the positive staining with fluorescein dye in Figure 6H (dotted line). An intact epithelial layer excluded the dye in the AM (Fig. 6F) and carrier-free (Fig. 6G) sheet transplants. The irregular staining in the AM sheet corresponds to folds in the transplant. Optical clarity was higher in the carrier-free group (Fig. 6D) than in the group with AM sheet transplants (Fig. 6C). Rabbits in the AM sheet group also had inflammation of the conjunctiva due to the presence of sutures. The area of intact epithelium at 1 week after surgery was significantly higher in both AM (79.4% ± 20.4%) and carrier-free (90.7% ± 17.4%) epithelial sheet groups compared with the sham-surgery control (40.2% ± 18.3%, $P < 0.05$; Fig. 6I).

Immunohistochemistry of postoperative corneas showed normal K3 expression in the transplant sheets (Figs. 7C, 7D). Sham-surgery eyes exhibited partial epithelialization by K3-negative epithelium of conjunctival origin. Basement membrane components such as collagen IV were more prominent in the AM sheet group (Figs. 7E, 7F). Proliferation of transplanted cells was observed by the distribution of BrdU staining, which was uniformly present in cells before surgery. BrdU-positive cells were observed in both groups, indicating that these cells were of donor origin and were slow cycling during the 1-week period after surgery (Figs. 7G, 7H). The number of BrdU-positive cells in the AM group was significantly higher

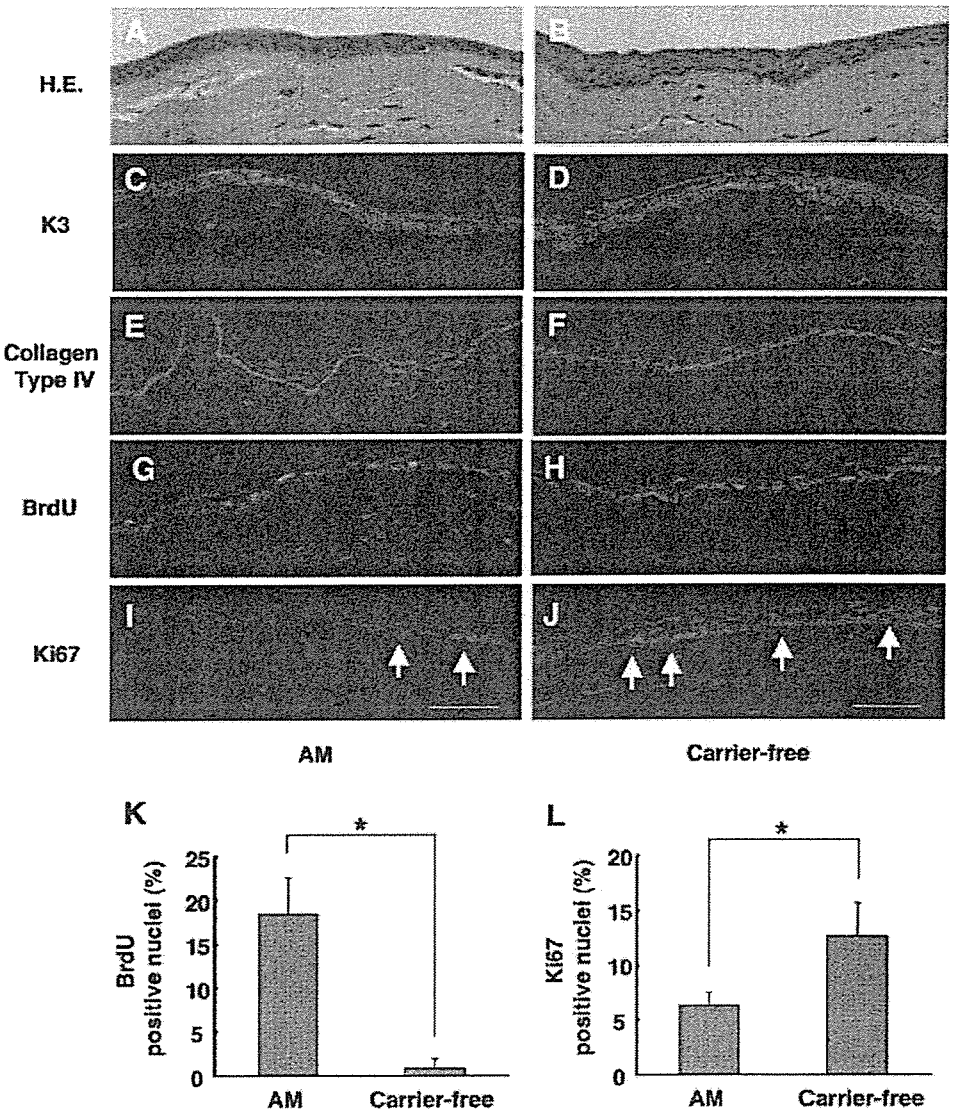

FIGURE 7. Postoperative histology of epithelial sheet transplantation. Light micrograph of hematoxylin and eosin–stained sections of AM (A) and carrier-free (B) epithelial sheets. Immunohistochemistry of K3 (C, D), Collagen type IV (E, F), BrdU (G, H), and Ki67 (I, J). AM sheets retained significantly higher levels of BrdU (K) and expressed lower levels of Ki67 (L) than did carrier-free sheets (*$P < 0.05$, Student's t-test). Scale bar, 50 μm.

than that in the fibrin group (AM: 18.4% ± 4.2%, fibrin: 1.1% ± 1.1%, $P = 0.0002$, $n = 4$; Fig. 7K). Staining of the proliferation marker Ki67 was also observed in the basal layers of both groups (Figs. 7I, 7J), with significantly less Ki67-positive cells in the AM group than in the fibrin group (AM: 6.3% ± 1.2%, fibrin: 12.6% ± 3.1%, $P = 0.0087$, $n = 4$; Fig. 7L). BrdU- and Ki67-positive cells were uniformly distributed throughout the epithelial sheet in both groups, and there was no tendency of higher localization of label retaining cells in the limbus under the conditions of the study.

DISCUSSION

The homeostasis of cells undergoing constant turnover depends on the healthy supply of regenerating cells, as well as an intact interaction between surrounding tissues. In the case of the corneal epithelium, stem cells in the basal limbus supply transient amplifying (TA) cells to the corneal basal layer, which proliferate and slough off the ocular surface after approximately 2 weeks. The proliferation and differentiation of epithelial cells is regulated by stromal–epithelial interaction with keratocytes, the major mesenchymal cell in the corneal stroma. Chemokines and growth factors secreted by keratocytes are involved in the proliferation and differentiation of the overlying epithelium.[17] We found that although both AM sheets and carrier-free sheets were viable in transplant-recipient eyes, carrier-free transplants demonstrated a more robust layer of fully differentiated cells.

We observed more BrdU labeled cells and fewer Ki67-labeled cells in AM sheets compared with carrier-free sheets after transplantation. Previous studies have shown that cell-cycle kinetics and cell phenotype characteristic of limbal epithelial progenitor cells are preserved during ex vivo expansion on AM.[18,19] The difference in cell-cycle kinetics may be due to the presence of the AM basement membrane, which may modulate epithelial cell adhesion, proliferation, and differentiation.[18,20,21] In contrast, epithelial cells in carrier-free sheets seem to become integrated into the host tissue earlier, suggesting that the AM may be interfering with interactions between the epithelium and stromal cells. The absence of a carrier will restore epithelium–stromal interactions immediately after surgery, may have several advantages in maintaining a healthy epithelium, and may also allow the regeneration of a normal subepithelial nerve plexus. It can be argued that a larger yield of undifferentiated cells may be preferable in the treatment of stem cell–depleted cases. However, a mature corneal epithe-

lium is also required for the ocular surface to act as a barrier against invading organisms, as well as to provide a smooth surface for visual clarity. The clinical data available to date show that both AM sheets and carrier-free sheets can restore the epithelium for more than 1 year,[7,9] which would not be possible without the restoration of progenitor cells.

Another major benefit of carrier-free cell sheets is the surgical technique, which does not require the use of sutures for donor fixation. The mechanisms involved may be multiple, however, Nishida et al.[8] show that intact basement membrane substrates and adhesion molecules may play a major role. We have confirmed the presence of $\beta 1$ integrin in the carrier-free group, which may have aided the carrier-free sheets in remaining on the ocular surface without sloughing off. In contrast, AM sheets require sutures for transplantation, and ingrowth of cells was observed under the AM carrier in several cases. These results show that attachment of cell sheets to the underlying stroma is stronger with carrier-free sheets during the early postoperative stage. Furthermore, the method we describe for engineering carrier-free sheets is different from previous approaches involving temperature-responsive dishes and does not require any specialized equipment or high levels of technical expertise.

The design of our study made use of rabbits with denuded epithelium, including the limbal area. We did not take into account any damage to the underlying stromal tissue, which is sometimes observed in clinical cases after severe chemical and thermal burns. The conclusions drawn from our study therefore should be interpreted as being based on epithelial sheet transplantation in situations with relatively intact stromal tissue. The AM is rich in basement membrane components since the amnion itself supports epithelial cells in the uterus. The use of an AM carrier may therefore have benefits in cases with extensive damage and inflammation in the underlying stroma.

There are still several issues to be resolved before the generalization of epithelial sheet surgery. The manufacture of stratified epithelial sheets requires the use of 3T3 feeder cells and culture-grade serum. Although adverse effects have not been reported, xeno-free techniques should be pursued. Similarly, the choice of whether to use carriers or not requires elucidation. Our data clearly show that cell sheets engineered without carriers reconstruct host tissue nearly to its original state as early as 1 week after surgery. Further refinements in surgical technique and quality control of cultured sheets should expand the therapeutic indications for tissue-engineered cell sheet transplantation.

Acknowledgments

The authors thank Mifuyu Oshima and Tomomi Sekiguchi for technical assistance and the staff of the Cornea Center Eye Bank for administrative support.

References

1. Kenyon KR, Tseng SC. Limbal autograft transplantation for ocular surface disorders. *Ophthalmology.* 1989;96:709–722; discussion 722–723.
2. Tsubota K, Satake Y, Kaido M, et al. Treatment of severe ocular-surface disorders with corneal epithelial stem-cell transplantation. *N Engl J Med.* 1999;340:1697–1703.
3. Pellegrini G, Traverso CE, Franzi AT, et al. Long-term restoration of damaged corneal surfaces with autologous cultivated corneal epithelium. *Lancet.* 1997;349:990–993.
4. Rama P, Bonini S, Lambiase A, et al. Autologous fibrin-cultured limbal stem cells permanently restore the corneal surface of patients with total limbal stem cell deficiency. *Transplantation.* 2001;72:1478–1485.
5. Koizumi N, Inatomi T, Quantock AJ, et al. Amniotic membrane as a substrate for cultivating limbal corneal epithelial cells for autologous transplantation in rabbits. *Cornea.* 2000;19:65–71.
6. Tsai RJ, Li LM, Chen JK. Reconstruction of damaged corneas by transplantation of autologous limbal epithelial cells. *N Engl J Med.* 2000;343:86–93.
7. Shimazaki J, Aiba M, Goto E, et al. Transplantation of human limbal epithelium cultivated on amniotic membrane for the treatment of severe ocular surface disorders. *Ophthalmology.* 2002;109:1285–1290.
8. Nishida K, Yamato M, Hayashida Y, et al. Functional bioengineered corneal epithelial sheet grafts from corneal stem cells expanded ex vivo on a temperature-responsive cell culture surface. *Transplantation.* 2004;77:379–385.
9. Nishida K, Yamato M, Hayashida Y, et al. Corneal reconstruction with tissue-engineered cell sheets composed of autologous oral mucosal epithelium. *N Engl J Med.* 2004;351:1187–1196.
10. Nakamura T, Endo K, Cooper LJ, et al. The successful culture and autologous transplantation of rabbit oral mucosal epithelial cells on amniotic membrane. *Invest Ophthalmol Vis Sci.* 2003;44:106–116.
11. Nakamura T, Inatomi T, Sotozono C, et al. Transplantation of cultivated autologous oral mucosal epithelial cells in patients with severe ocular surface disorders. *Br J Ophthalmol.* 04;88:1280–1284.
12. Itabashi Y, Miyoshi S, Kawaguchi H, et al. A new method for manufacturing cardiac cell sheets using fibrin-coated dishes and its electrophysiological studies by optical mapping. *Artif Organs.* 2005;29:95–103.
13. Espana EM, Romano AC, Kawakita T, et al. Novel enzymatic isolation of an entire viable human limbal epithelial sheet. *Invest Ophthalmol Vis Sci.* 2003;44:4275–4281.
14. Kim HS, Jun Song X, de Paiva CS, et al. Phenotypic characterization of human corneal epithelial cells expanded ex vivo from limbal explant and single cell cultures. *Exp Eye Res.* 2004;79:41–49.
15. Li DQ, Chen Z, Song XJ, et al. Partial enrichment of a population of human limbal epithelial cells with putative stem cell properties based on collagen type IV adhesiveness. *Exp Eye Res.* 2005;80:581–590.
16. Tseng SC, Kruse FE, Merritt J, Li DQ. Comparison between serum-free and fibroblast-cocultured single-cell clonal culture systems: evidence showing that epithelial anti-apoptotic activity is present in 3T3 fibroblast-conditioned media. *Curr Eye Res.* 1996;15:973–984.
17. Wilson SE, Mohan RR, Mohan RR, et al. The corneal wound healing response: cytokine-mediated interaction of the epithelium, stroma, and inflammatory cells. *Prog Retin Eye Res.* 2001;20:625–637.
18. Grueterich M, Espana E, Tseng SC. Connexin 43 expression and proliferation of human limbal epithelium on intact and denuded amniotic membrane. *Invest Ophthalmol Vis Sci.* 2002;43:63–71.
19. Meller D, Pires RT, Tseng SC. Ex vivo preservation and expansion of human limbal epithelial stem cells on amniotic membrane cultures. *Br J Ophthalmol.* 2002;86:463–471.
20. Jones PH, Harper S, Watt FM. Stem cell patterning and fate in human epidermis. *Cell.* 1995;80:83–93.
21. Li W, He H, Kuo CL, et al. Basement membrane dissolution and reassembly by limbal corneal epithelial cells expanded on amniotic membrane. *Invest Ophthalmol Vis Sci.* 2006;47:2381–2389.

Available online at www.sciencedirect.com
ScienceDirect
Biochemical and Biophysical Research Communications 350 (2006) 315–321
BBRC
www.elsevier.com/locate/ybbrc

Loss of HB-EGF in smooth muscle or endothelial cell lineages causes heart malformation

Daisuke Nanba [a,1], Yumi Kinugasa [a,1], Chie Morimoto [a], Michiko Koizumi [a], Hisako Yamamura [c], Katsuhito Takahashi [c], Nobuyuki Takakura [d], Eisuke Mekada [e], Koji Hashimoto [b], Shigeki Higashiyama [a,f,*]

[a] *Department of Biochemistry and Molecular Genetics, Ehime University Graduate School of Medicine, Shitsukawa, To-on, Ehime 791-0295, Japan*
[b] *Department of Dermatology, Ehime University Graduate School of Medicine, Shitsukawa, To-on, Ehime 791-0295, Japan*
[c] *Department of Medicine, Osaka Medical Center for Cancer and Cardiovascular Diseases, Osaka 537-8511, Japan*
[d] *Department of Signal Transduction, Research Institute for Microbial Diseases, Osaka University, Osaka 565-0871, Japan*
[e] *Department of Cell Biology, Research Institute for Microbial Diseases, Osaka University, Osaka 565-0871, Japan*
[f] *PRESTO, JST, Japan*

Received 22 August 2006
Available online 22 September 2006

Abstract

Epidermal growth factor (EGF) and ErbB family molecules play a role in heart development and function. To investigate the role of EGF family member, heparin-binding EGF-like growth factor (HB-EGF) in heart development, smooth muscle and endothelial cell lineage-specific HB-EGF knockout mice were generated using the Cre/*loxP* system in combination with the *SM22α* or *TIE2* promoter. HB-EGF knockout mice displayed enlarged heart valves, and over half of these mice died during the first postnatal week, while survivors showed cardiac hypertrophy. These results suggest that expression of HB-EGF in smooth muscle and/or endothelial cell lineages is essential for proper heart development and function in mice.

Keywords: Cardiac hypertrophy; Conditional knockout; HB-EGF; Heart valves; Heart failure

Heparin-binding EGF-like growth factor (HB-EGF) is a member of the EGF family of molecules that was first identified in the conditioned media of macrophage-like U-937 cells [1]. HB-EGF is initially synthesized as a type I transmembrane precursor protein (proHB-EGF) that is subsequently enzymatically cleaved to release a soluble form of HB-EGF [1,2]. Further, HB-EGF acts as a mitogen in many different cell types and is involved in a variety of physiological and pathological processes [3–5].

Two independent studies have reported that over half of HB-EGF-null mice die before weaning and that survivors have dysfunctional hearts with grossly enlarged ventricular chambers and reduced life spans [6,7]. Moreover, studies have described the development of enlarged cardiac valves in HB-EGF-deficient mice. This heart valve enlargement has also been observed in EGF receptor (EGFR)-null mice with a CD1 background, in mice with a mutant EGFR (*waved-2*) [8], and in disintegrin and metalloprotease (ADAM) 17-null mice [7], which is a sheddase of proHB-EGF [9,10]. These results indicate that ectodomain shedding of proHB-EGF and subsequent EGFR activation induced by released HB-EGF are crucial for heart valve formation in developmental process as well as development of cardiac hypertrophy in pathological process [11]. However, it is not clear in which of the specific heart cell types (e.g., cardiac myocytes, endothelial cells, and fibroblasts) that HB-EGF expression is required for proper heart development and function.

* Corresponding author. Fax: +81 89 960 5256.
E-mail address: shigeki@m.ehime-u.ac.jp (S. Higashiyama).
[1] These authors contributed equally to this work.

0006-291X/$ - see front matter © 2006 Elsevier Inc. All rights reserved.
doi:10.1016/j.bbrc.2006.09.060

To address this issue, the present study utilized the Cre/*loxP* recombination system for spatiotemporal *HB-EGF* gene ablation. The system generally requires cross-mating of two lines of genetically manipulated mice. One line of mice carries alleles with the *HB-EGF* gene flanked by *loxP* sites [6], and the other line contains a Cre transgene in which the expression of Cre is controlled by *SM22α* or *TIE2* promoter [12,13]. Recombination between the two *loxP* sites in the mated mice results in the catalysis of a deletion of the region flanked by the *loxP* sites (i.e., Cre-dependent transgene expression).

The *SM22α* gene encodes a calponin-related protein that is expressed specifically in adult smooth muscle [14–17]. During mouse embryogenesis, *SM22α* is expressed in cardiac muscle, smooth muscle, and skeletal muscle cells, but becomes restricted to smooth muscle lineages at late embryonic stages and throughout adulthood [18]. The *TIE2* gene encodes an angiopoietin receptor, which is a member of the receptor tyrosine kinase family [19,20]. *TIE2* expression is detected as the first endothelial cells arise, remains positive in endothelial cells throughout development, and is detectable in virtually all endothelial cells of adult tissues [19,21,22].

In this study, we generated smooth muscle and endothelial cell lineage specific HB-EGF knockout mice using Cre/*loxP* system in combination with the *SM22α* and *TIE2* promoter, and demonstrated that HB-EGF in smooth muscle and endothelial lineages was essential for heart development and function.

Materials and methods

Generation of HB-EGF conditional knockout mice using a gene targeting Cre/loxP strategy. Mice with *HB-EGF* gene flanked by *loxP* sites ($HB^{lox/lox}$) were generated as previously described [6]. Homozygous $HB^{lox/lox}$ mice were bred with *SM22α* or *TIE2* promoter-driven Cre-recombinase transgenic mice [12,13] to generate SM22α-Cre:$HB^{lox/WT}$ or TIE2-Cre:$HB^{lox/WT}$ mice. The obtained mice were bred with $HB^{lox/lox}$ mice to generate SM22α-Cre:$HB^{lox/lox}$ (SM22α-Cre:$HB^{-/-}$) or TIE2-Cre:$HB^{lox/lox}$ (TIE2-Cre:$HB^{-/-}$) mice. The genotype of each mouse was confirmed by PCR. Primers are shown in Table 1.

Table 1
Primer sequences for PCR

Wild-type *HB-EGF* (forward)	5′-CATGATGCTCCAGTGAGTAGGCTCTGATTAC-3′
Wild-type *HB-EGF* (reverse)	5′-AGGGCAAGATCATGTGTCCTGCCTCAAGCC-3′
loxP HB-EGF (forward)	5′-ATGGGATCGGCCATTGAACA-3′
loxP HB-EGF (reverse)	5′-GAAGAACTCGTCAAGAAGGC-3′
Cre recombinase (forward)	5′-TTACCGGTCGATGCAACGAGTGATG-3′
Cre recombinase (reverse)	5′-TTCCATGAGTGAACGAACCTGGTCG-3′
SM22α promoter Cre (forward)	5′-CCAGAGAACAGTGAAGTAGGAG-3′
SM22α promoter Cre (reverse)	5′-CATCCAGTCTTGCGAACCTCAT-3′
TIE2 promoter Cre (forward)	5′-CCCTGTGCTCAGACAGAAATGAGA-3′
TIE2 promoter Cre (reverse)	5′-CGCATAACCAGTGAAACAGCATTGC-3′

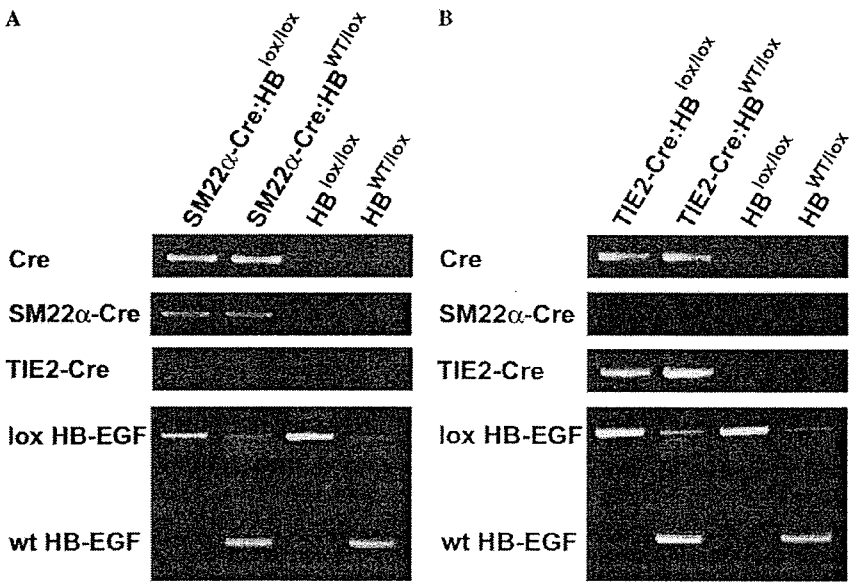

Fig. 1. Genotypes of the conditional knockout mice. SM22α-Cre:$HB^{lox/lox}$ (A) and TIE2-Cre:$HB^{lox/lox}$ (B) mice were confirmed by PCR. *SM22α*-Cre but not *TIE2*-Cre transgenes were detected with SM22α-Cre specific primers and vice versa. The *HB-EGF* gene flanked by *loxP* sites and the wild-type gene were also confirmed by PCR genotyping.

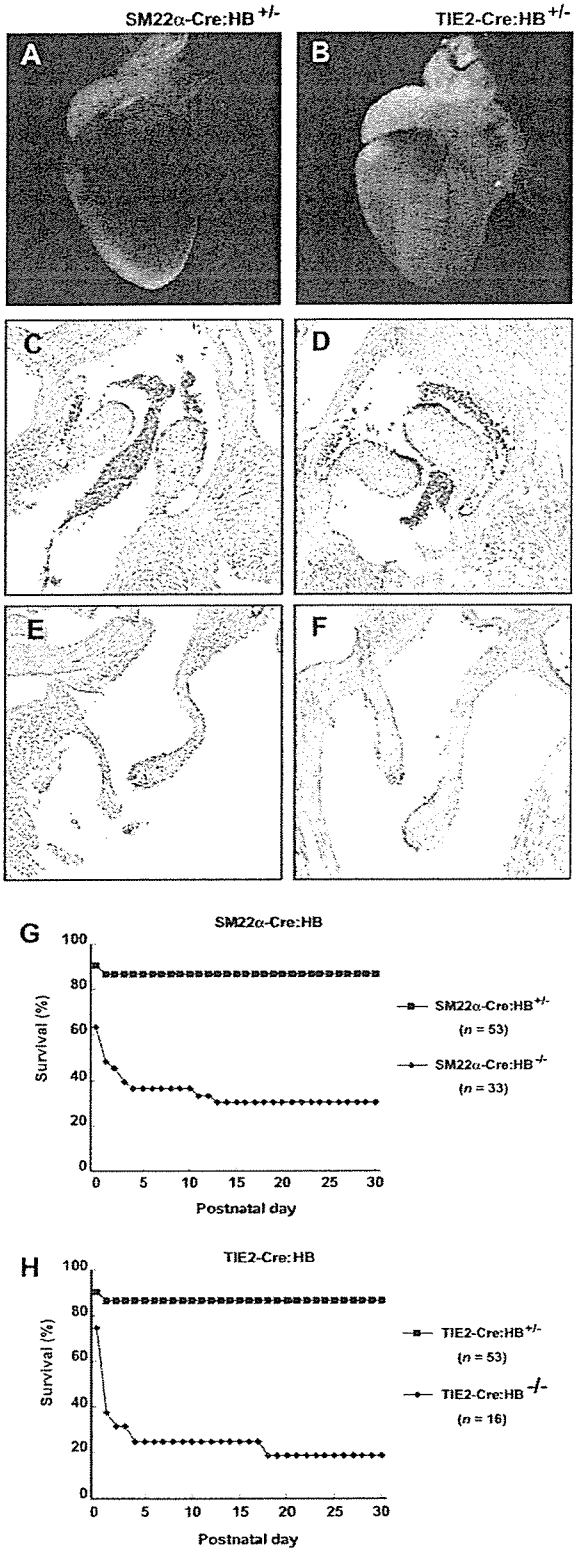

Histological analysis. Mouse tissues were fixed in 3.7% formaldehyde, dehydrated, and embedded in paraffin. Ten micrometer sections were stained with hematoxylin and eosin. For X-gal staining, after fixation with 2% formaldehyde and 0.2% glutaraldehyde, the tissues were stained with 5-bromo-4-chloro-3-indolyl β-D-galactoside (X-Gal). The stained tissues were fixed again with 3.7% formaldehyde, dehydrated, and embedded in paraffin. Ten micrometer sections were stained with eosin.

Results

Generation of HB-EGF conditional knockout mice

To generate cell-type specific HB-EGF knockout mice, mice carrying alleles with the *HB-EGF* gene flanked by *loxP* sites ($HB^{lox/lox}$; [6]) were crossed with SM22α-Cre [12] or TIE2-Cre [13] transgenic mice. The obtained mice carrying the wild-type and *loxP HB-EGF* genes, and Cre transgenes (SM22α-Cre:$HB^{WT/lox}$ or TIE2-Cre:$HB^{WT/lox}$, which we refer to as SM22α-Cre:$HB^{+/-}$ or TIE2-Cre:$HB^{+/-}$) were bred again with $HB^{lox/lox}$ mice to generate SM22α-Cre:$HB^{lox/lox}$ or TIE2-Cre:$HB^{lox/lox}$ mice, which we refer to as SM22α-Cre:$HB^{-/-}$ or TIE2-Cre:$HB^{-/-}$ mice. The genotype of mice was confirmed by PCR analysis (Fig. 1). No overt abnormalities were observed in $HB^{WT/lox}$ or $HB^{lox/lox}$ mice [6,23], and there was no evidence that strong expression of Cre recombinase induced abnormalities in wild-type mice.

HB-EGF expression in the heart of HB-EGF conditional knockout mice

The targeting vector used for the generation of $HB^{lox/lox}$ mice contains the *lacZ* reporter gene under the control of the native *HB-EGF* promoter, which is activated by Cre-mediated recombination [6]. Beta-gal staining of newborn (postnatal day 1; P1) hearts in SM22α-Cre:$HB^{+/-}$ and TIE2-Cre:$HB^{+/-}$ mice showed that HB-EGF was strongly expressed at the site where the great vessels and coronary arteries arise from the heart (Fig. 2A and B). Histological analysis of the heart revealed that β-gal positive cells were localized to the margins of all of the heart valves, including the semilunar (aortic and pulmonic) valves (Fig. 2C and D) and the atrioventricular (mitral and tricuspid) valves (Fig. 2E and F). These results indicate that HB-EGF expression was blocked in the endocardium of the heart valves and the coronary artery of SM22α-Cre:$HB^{-/-}$ and TIE2-Cre:$HB^{-/-}$ mice.

Fig. 2. The heart morphologies and the tissue sections of newborn (P1) SM22α-Cre:$HB^{+/-}$ and TIE2-Cre:$HB^{+/-}$ (corresponds to wild-type) mice and survival of conditional knockout mice. Whole mount β-gal staining revealed that HB-EGF was strongly expressed at sites at which the great vessels and coronary arteries arise from the heart in SM22α-Cre:$HB^{+/-}$ (A) and TIE2-Cre:$HB^{+/-}$ (B) mice. The longitudinal sections showed that HB-EGF was expressed at the margin of the semilunar (C; SM22α-Cre:$HB^{+/-}$ and D; TIE2-Cre:$HB^{+/-}$) and atrioventricular (E; SM22α-Cre:$HB^{+/-}$ and F; TIE2-Cre:$HB^{+/-}$) valves. Over half of the SM22α-Cre:$HB^{-/-}$ (G) and TIE2-Cre:$HB^{-/-}$ (H) mice died within the first day after birth. Approximately 70–80% of these knockout mice died with the first 2 weeks after birth.

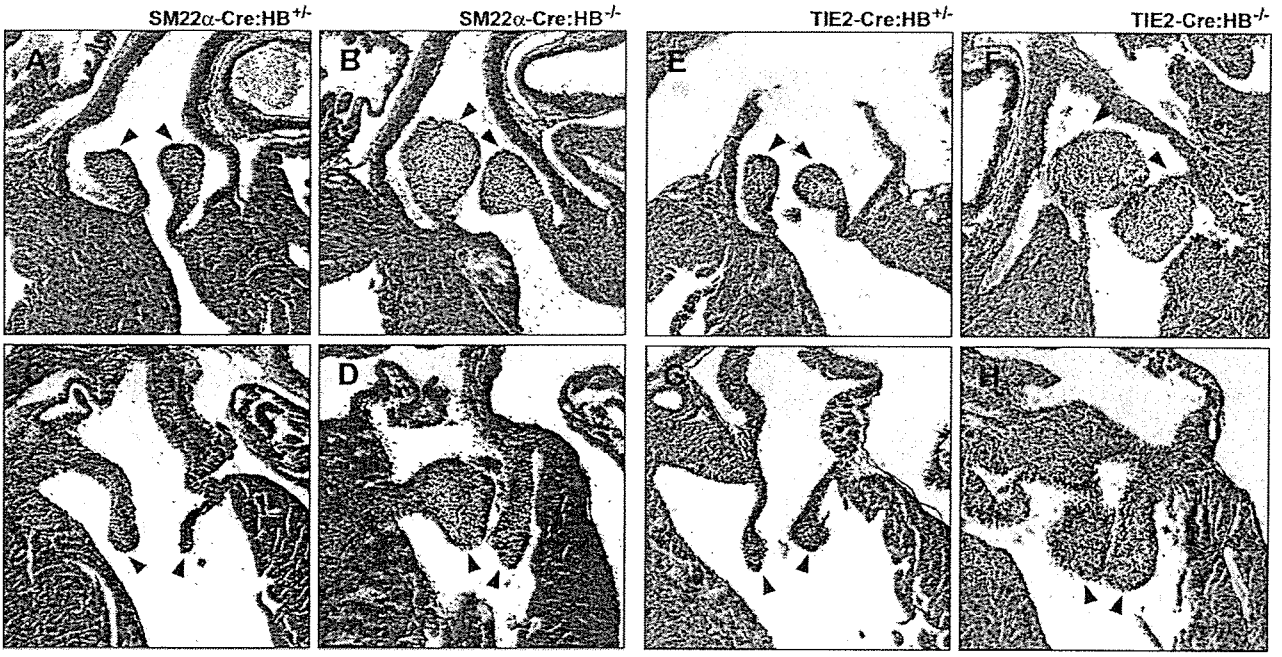

Fig. 3. Hematoxylin and eosin staining of the longitudinal sections of the newborn (P1) heart valves. Histological sections show semilunar (A, B, E and F) and atrioventricular (C, D, G and H) valves. In SM22α-Cre:$HB^{-/-}$ (B and D) and TIE2-Cre:$HB^{-/-}$ (F and H) mice, the valves were enlarged when compared with SM22α-Cre:$HB^{+/-}$ (A and C) and TIE2-Cre:$HB^{+/-}$ (E and G) mice. The valves are indicated with arrowheads.

Postnatal lethality of HB-EGF conditional knockout

Breeding of SM22α-Cre:$HB^{WT/lox}$ or TIE2-Cre:$HB^{WT/lox}$ with homozygous $HB^{lox/lox}$ mice yielded HB-EGF conditional knockout mice. Half of these mice died within one day after birth. Seventy percent of SM22α-Cre:$HB^{-/-}$ mice died within 13 days after birth (Fig. 2G), and 80% of TIE2-Cre:$HB^{-/-}$ mice died within 18 days after birth (Fig. 2H). SM22α-Cre:$HB^{-/-}$ and TIE2-Cre:$HB^{-/-}$ mice survivors displayed no obvious outward abnormalities and remained alive for at least several months after birth (data not shown).

Enlarged heart valves in HB-EGF conditional knockout mice

Histological analysis of newborn (P1) hearts revealed that SM22α-Cre:$HB^{-/-}$ and TIE2-Cre:$HB^{-/-}$ mice developed enlarged semilunar (Fig. 3A, B, E and F) and atrioventricular (Fig. 3C, D, G and H) valves when compared with SM22α-Cre:$HB^{+/-}$ and TIE2-Cre:$HB^{+/-}$ mice. This phenotype was consistent with that of HB-EGF-null mice [6,7]. The enlargement of neonatal heart in HB-EGF-deficient mice [6,7], however, was not observed in the P1 heart of these conditional knockout mice (data not shown).

Cardiac hypertrophy in HB-EGF conditional knockout mice

Although the survivors of SM22α-Cre:$HB^{-/-}$ and TIE2-Cre:$HB^{-/-}$ mice initially appeared normal, massive enlargement of the heart was apparent by 12 weeks of age when compared with control mice (Fig. 4A–D). Specifically, the mean heart-to-body wet weight ratio was $1.64 \pm 0.74\%$ for 12-week-old SM22α-Cre:$HB^{-/-}$ mice and was $0.65 \pm 0.16\%$ for 12-week-old SM22α-Cre:$HB^{+/-}$ mice (Fig. 4E). Further, the mean ratio of heart/body weight was $1.36 \pm 0.48\%$ for 12-week-old TIE2-Cre:$HB^{-/-}$ mice and was $0.76 \pm 0.063\%$ for 12-week-old TIE2-Cre:$HB^{+/-}$ mice (Fig. 4F).

Discussion

The present study demonstrated that loss of HB-EGF in smooth muscle or endothelial cell lineages resulted in heart valve malformations, postnatal lethality, and cardiac hypertrophy, which is a phenotype similar to that of HB-EGF-null mice [6,7]. The *HB-EGF* gene was deleted in endocardial cells of the heart valves in SM22α-Cre:$HB^{-/-}$ and TIE2-Cre:$HB^{-/-}$ mice. Data from the present study suggest that enlargement of the heart valves results from the loss of HB-EGF in the endocardial cells of heart valves, and the heart valve malformation is likely responsible for the postnatal lethality and cardiac hypertrophy of these *HB-EGF* conditional knockout mice.

Heart valves develop from endocardial cushions, which form when the endocardial cells undergo an endocardial-mesenchymal transition (EMT) and proliferate and invade the cardiac jelly, a basement membrane-like substance produced by the myocardial cells. The endocardial cushion area elongates and undergoes continuous remodeling to refine the primitive cushion into thin elongated valve leaflets.

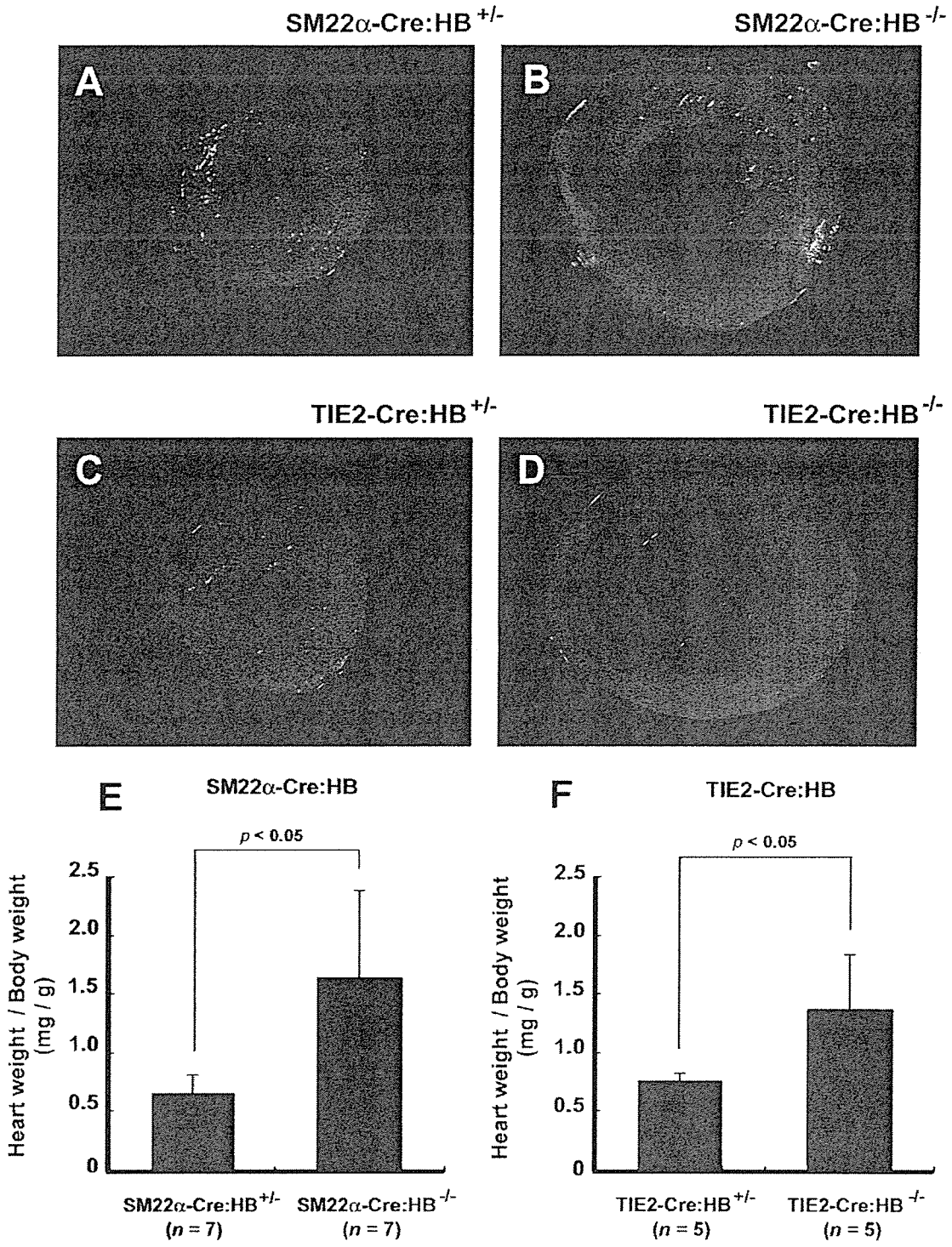

Fig. 4. Cardiac hypertrophy of the conditional knockout mice. Transverse sections of the hearts (A–D) and heart weight-to-body wet weight ratios (E and F) of 12-week-old mice. Values represent means ± SD. Massive enlargement of the heart was observed in SM22α-Cre:HB$^{-/-}$ and TIE2-Cre:HB$^{-/-}$ mice when compared with the control mice.

SM22α is expressed in cardiac muscle, smooth muscle, and skeletal muscle cells during embryogenesis, but becomes restricted to smooth muscle lineages at late embryonic stages and throughout adulthood [18]. Although HB-EGF is expressed in the heart [6,7], we could not detect obvious β-gal staining in myocardium of SM22α-Cre:HB$^{+/-}$ mice. *SM22α-lacZ* mice show the low expression of this transgene in myocardium during late development [24], which

suggests low *SM22α-Cre* activity and subsequent recombination efficiency with *loxP HB-EGF* in myocardium of SM22α-Cre:HB$^{+/-}$ mice. During early avian cardiac development, the endocardium-derived mesenchymal cells, which form endocardial cushions and subsequently form heart valves, have characteristics of smooth muscle-like myofibroblasts and express smooth muscle-specific alpha actin [25]. This finding suggests that the mesenchymal cells that had transformed from endocardial cells expressed the smooth muscle-specific *SM22α* gene, and this fact may account for *HB-EGF* gene deletion in the heart valves of SM22α-Cre:HB$^{-/-}$ mice.

TIE2 is expressed in endothelial cells throughout development [19,21,22]. Previous studies have reported that *TIE2*-Cre:R26R mice have β-galactosidase activity that was restricted to the endocardium and the mesenchyme of the endocardial cushions but was never observed in myocardium or epicardium of the developing heart [26]. These data indicate that the *HB-EGF* gene was eliminated in endocardial but not in myocardial cell lineages in the developing heart of TIE2-Cre:HB$^{-/-}$ mice. Therefore, the present study suggests that the loss of endocardial but not myocardial HB-EGF is at least responsible for the heart valve enlargement in HB-EGF-null mice.

Enlargement of heart valves has also been observed in mutant mice expressing an uncleavable form of proHB-EGF [27], in ADAM17-null mice [7], in EGFR-null mice with a CD1 background, and in mice expressing a mutant EGFR (*waved-2*) [8]. Together with data from the present study, these observations indicate that ectodomain shedding of proHB-EGF in endocardial cells of heart valves and subsequent EGFR activation are essential for remodeling of endocardial cushions. Although the mechanism of cushion remodeling is largely unknown, HB-EGF/EGFR signaling in the mesenchymal cells within the endocardial cushions may suppress cellular proliferation to refine the primitive cushion into thin elongated valve leaflets [7,28]. Recent studies have reported that the cytoplasmic domain of proHB-EGF and C-terminal fragment of proHB-EGF generated by ectodomain shedding have some functions [29–31]. These intracellular signaling might be involved in the heart valve formation.

In conclusion, the loss of *HB-EGF* gene expression in smooth muscle or endothelial cell lineages of the developing mouse results in heart valve malformations and cardiac hypertrophy. These data indicate the significance of endocardial HB-EGF for proper heart development and function.

Acknowledgments

This work is supported by Grants-in-Aid for Scientific Research (No. 17390081) to S.H. from the Ministry of Education, Culture, Sports, Science and Technology of Japan, and Precursory Research for Embryonic Science and Technology (Information and Cell Function).

References

[1] S. Higashiyama, J.A. Abraham, J. Miller, J.C. Fiddes, M. Klagsbrun, A heparin-binding growth factor secreted by macrophage-like cells that is related to EGF, Science 251 (1991) 936–939.
[2] S. Higashiyama, K. Lau, G. Besner, J.A. Abraham, M. Klagsbrun, Structure of heparin-binding EGF-like growth factor: multiple forms, primary structure, and glycosilation of the mature protein, J. Biol. Chem. 267 (1992) 6205–6212.
[3] R. Iwamoto, E. Mekada, Heparin-binding EGF-like growth factor: a juxtacrine growth factor, Cytokine Growth Factor Rev. 11 (2000) 335–344.
[4] E. Nishi, M. Klagsbrun, Heparin-binding epidermal growth factor-like (HB-EGF) is a mediator of multiple physiological and pathological pathways, Growth factors 22 (2004) 253–260.
[5] S. Higashiyama, D. Nanba, ADAM-mediated ectodomain shedding of HB-EGF in receptor cross-talk, Biochim. Biophys. Acta. 1751 (2005) 110–117.
[6] R. Iwamoto, S. Yamazaki, M. Asakura, S. Takashima, H. Hasuwa, K. Miyado, S. Adachi, M. Kitakaze, K. Hashimoto, G. Raab, D. Nanba, S. Higashiyama, M. Hori, M. Klagsbrun, E. Mekada, Heparin-binding EGF-like growth factor and ErbB signaling is essential for heart function, Proc. Natl. Acad. Sci. USA 100 (2003) 3221–3226.
[7] L.F. Jackson, T.H. Qiu, S.W. Sunnarborg, A. Chang, C. Zhang, S. Patterson, D.C. Lee, Defective valvulogenesis in HB-EGF and TACE-null mice is associated with aberrant BMP signaling, EMBO J. 22 (2003) 2704–2716.
[8] B. Chen, R.T. Bronson, L.D. Klaman, T.G. Hampton, J.F. Wang, P.J. Green, T. Magnouson, P.S. Douglas, J.P. Morgan, B.G. Neel, Mice mutant for Egfr and Shp2 have defective cardiac semilunar valvulogenesis, Nat. Genet. 24 (2000) 96–299.
[9] S.W. Sunnarborg, C.L. Hinkle, M. Stevenson, W.E. Russell, C.S. Raska, J.J. Peschon, B.J. Castner, M.J. Gerhart, R.J. Paxton, R.A. Black, D.C. Lee, Tumor necrosis factor-alpha converting enzyme (TACE) regulates epidermal growth factor receptor ligand availability, J. Biol. Chem. 277 (2002) 12838–12845.
[10] U. Sahin, G. Weskamp, K. Kelly, H. Zhou, S. Higashiyama, J. Peschon, D. Hartmann, P. Saftig, C.P. Blobel, Distinct roles for ADAM10 an ADAM17 in ectodomain shedding of six EGFR ligands, J. Cell Biol. 164 (2004) 769–779.
[11] M. Asakura, M. Kitakaze, S. Takashima, Y. Liao, F. Ishikura, T. Yoshinaka, H. Ohmoto, K. Node, K. Yoshino, H. Ishiguro, H. Asanuma, S. Sanada, Y. Matsumura, H. Takeda, S. Beppu, M. Tada, M. Hori, S. Higashiyama, Cardiac hypertrophy is inhibited by antagonism of ADAM12 processing of HB-EGF: metalloproteinase inhibitors as a new therapy, Nature Med. 8 (2002) 35–40.
[12] R. Holtwick, M. Gotthardt, B. Skryabin, M. Steinmetz, R. Potthast, B. Zetsche, R.E. Hammer, J. Herz, M. Kuhn, Smooth muscle-selective deletion of guanylyl cyclase-A prevents the acute but not chronic effects of ANP on blood pressure, Proc. Natl. Acad. Sci. USA 99 (2002) 7142–7147.
[13] P.A. Koni, S.K. Joshi, U.A. Temann, D. Olson, L. Burkly, RA. Flavell, Conditional vascular cell adhesion molecule 1 deletion in mice: impaired lymphocyte migration to bone marrow, J. Exp. Med. 193 (2001) 741–754.
[14] J.P. Lee-Miller, D.H. Heeley, L.B. Smillie, An abundant and novel protein of 22 kDa (SM22) is widely distributed in smooth muscles: purification from bovine aorta, Biochem. J. 244 (1987) 705–709.
[15] S.J. Winder, C. Sutherland, M.P. Walsh, Biochemical and functional characterization of smooth muscle calponin, Adv. Exp. Med. Biol. 304 (1991) 37–51.
[16] J.L. Duband, M. Gimona, M. Scatena, S. Sartore, J.V. Small, Calponin and SM 22 as differentiation markers of smooth muscle: spatiotemporal distribution during avian embryonic development, Differentiation 55 (1993) 1–11.

[17] W. Nishida, Y. Kitami, K. Hiwada, cDNA cloning and mRNA expression of calponin and SM22 in rat aorta smooth muscle cells, Gene 130 (1993) 297–302.
[18] L. Li, J.M. Miano, P. Cserjesi, E.N. Olson, SM22α, a marker of adult smooth muscle, is expressed in multiple myogenic lineages during embryogenesis, Circ. Res. 78 (1996) 188–195.
[19] T.N. Sato, Y. Qin, C.A. Kozak, K.L. Audus, Tie-1 and tie-2 define another class of putative receptor tyrosine kinase genes expressed in early embryonic vascular system, Proc. Natl. Acad. Sci. USA 90 (1993) 9355–9358.
[20] S. Davis, T.H. Aldrich, P.F. Jones, A. Acheson, D.L. Compton, V. Jain, T.E. Ryan, J. Bruno, C. Radziejewski, P.C. Maisonpierre, G.D. Yancopoulous, Isolation of angiopoietin-1, a ligand for the TIE2 receptor, by secretion-trap expressing cloning, Cell 87 (1996) 1161–1169.
[21] H. Schnürch, W. Risau, Expression of tie-2, a member of a novel family of receptor tyrosine kinases, in the endothelial cell lineage, Development 119 (1993) 957–968.
[22] A.L. Wong, Z.A. Haroon, S. Werner, M.W. Dewhirst, C.S. Greenberg, K.G. Peters, Tie2 expression and phosphorylation in angiogenic and quiescent adult tissues, Circ. Res. 81 (1997) 567–574.
[23] Y. Shirakata, R. Kimura, D. Nanba, R. Iwamoto, S. Tokumaru, C. Morimoto, K. Yokota, M. Nakamura, K. Sayama, E. Mekada, S. Higashiyama, K. Hashimoto, Heparin-binding EGF-like growth factor accelerates keratinocyte migration and skin wound healing, J. Cell Sci. 118 (2005) 2363–2370.
[24] L. Li, J.M. Miano, M. Mercer, E.N. Olson, Expression of the *SM22α* promoter in transgenic mice provides evidence for distinct transcriptional regulatory programs in vascular and visceral smooth muscle cells, J. Cell Biol. 132 (1996) 849–859.
[25] Y. Nakajima, V. Mironov, T. Yamagishi, H. Nakamura, R.R. Markwald, Expression of smooth muscle alpha-actin in mesenchymal cells during formation of avian endocardial cushion tissue: a role for transforming growth factor β3, Dev. Dyn. 209 (1997) 296–309.
[26] F.J. de Lange, A.F.M. Moorman, R.H. Anderson, J. Männer, A.T. Soufan, C. de Gier-de Vries, M.D. Schneider, S. Webb, M.J.B. van den Hoff, V.M. Christoffels, Lineage and morphogenetic analysis of the cardiac valves, Cir. Res. 95 (2004) 645–654.
[27] S. Yamazaki, R. Iwamoto, K. Saeki, M. Asakura, S. Takashima, A. Yamazaki, R. Kimura, H. Mizushima, H. Moribe, S. Higashiyama, M. Endoh, Y. Kaneda, S. Takagi, S. Itami, N. Takeda, G. Yamada, E. Mekada, Mice with defects in HB-EGF ectodomain shedding show severe developmental abnormarities, J. Cell Biol. 163 (2003) 469–475.
[28] R. Iwamoto, E. Mekada, ErbB and HB-EGF signaling in heart development and function, Cell Struct. Funct. 31 (2006) 1–14.
[29] J. Lin, L. Hutchinson, S.M. Gaston, G. Raab, M.R. Freeman, BAG-1 is a novel cytoplasmic binding partner of the membrane form of heparin-binding EGF-like growth factor: a unique role for proHB-EGF in cell survival regulation, J. Biol. Chem. 276 (2001) 30127–30132.
[30] D. Nanba, A. Mammoto, K. Hashimoto, S. Higashiyama, Proteolytic release of the carboxy-terminal fragment of proHB-EGF causes nuclear export of PLZF, J. Cell Biol. 163 (2003) 489–502.
[31] X. Wang, H. Mizushima, S. Adachi, M. Ohishi, R. Iwamoto, E. Makada, Cytoplasmic domain phosphorylation of heparin-binding EGF-likegrowth factor, Cell Struct. Funct. 31 (2006) 15–27.

Oncogene (2007) 26, 339–348

www.nature.com/onc

ORIGINAL ARTICLE

Pre-B-cell leukemia transcription factor 1 is a major target of promyelocytic leukemia zinc-finger-mediated melanoma cell growth suppression

K Shiraishi[1,2], K Yamasaki[2], D Nanba[1], H Inoue[1], Y Hanakawa[2], Y Shirakata[2], K Hashimoto[2] and S Higashiyama[1,3]

[1]Department of Biochemistry and Molecular Genetics, Ehime University Graduate School of Medicine, Shitsukawa, Toon, Ehime, Japan; [2]Department of Dermatology, Ehime University Graduate School of Medicine, Shitsukawa, Toon, Ehime, Japan and [3]Precursory Research for Embryonic Science and Technology (PRESTO), Japan Science and Technology Corporation (JST), Kawaguchi City, Saitama, Japan

Promyelocytic leukemia zinc-finger (PLZF) is a transcriptional repressor and tumor suppressor. PLZF is expressed in melanocytes but not in melanoma cells, and recovery of PLZF expression markedly suppresses melanoma cell growth. Several target genes regulated by PLZF have been identified, but the precise function of PLZF remains uncertain. Here, we searched for candidate target genes of PLZF by DNA microarray analysis. Pre-B-cell leukemia transcription factor 1 (Pbx1) was one of the prominently suppressed genes. Pbx1 was highly expressed in melanoma cells, and its expression was reduced by transduction with the PLZF gene. Moreover, the growth suppression mediated by PLZF was reversed by enforced expression of Pbx1. Knockdown of Pbx1 by specific small interfering RNAs suppressed melanoma cell growth. We also found that Pbx1 binds HoxB7. Reverse transcription–polymerase chain reaction analysis demonstrated that repression of Pbx1 by PLZF reduces the expression of HoxB7 target genes, including tumor-associated neoangiogenesis factors such as basic fibroblast growth factor, angiopoietin-2 and matrix metalloprotease 9. These findings suggest that deregulation of Pbx1 expression owing to loss of PLZF expression contributes to the progression and/or pathogenesis of melanoma.
Oncogene (2007) **26,** 339–348. doi:10.1038/sj.onc.1209800; published online 24 July 2006

Keywords: Pbx1; PLZF; Hox; melanoma

Introduction

Malignant melanoma is a highly aggressive neoplastic disease whose incidence is increasing rapidly. To develop new therapies, it is essential to elucidate the molecular mechanisms by which melanocytes are transformed into malignant melanoma cells. A recent report found that the promyelocytic leukemia zinc-finger (PLZF) protein is expressed in melanocytes but not in melanoma cells, and that melanoma growth is markedly suppressed by enforced expression of PLZF (Felicetti *et al.*, 2004).

PLZF was first identified by its translocation with retinoic acid receptor alpha in t(11;17) acute promyelocytic leukemia (Chen *et al.*, 1993). The PLZF protein is a sequence-specific transcription repressor characterized by a BTB/POZ domain, which is responsible for transcriptional repression, and nine zinc-finger domains that form the DNA-binding domain (Hong *et al.*, 1997; Li *et al.*, 1997; Wong and Privalsky, 1998). Some target genes regulated by PLZF have been identified. Studies of PLZF-knockout mice indicate that PLZF represses HoxD gene expression through chromatin remodeling, which in turn regulates limb and axial skeletal patterning (Barna *et al.*, 2000, 2002). PLZF also binds to and represses the cyclin A2 promoter, and is involved in the regulation of cell cycle progression (Yeyati *et al.*, 1999). Moreover, PLZF represses c-*myc* expression, which is central to the control of cellular proliferation, apoptosis and differentiation (McConnell *et al.*, 2003). DNA microarray analyses have also revealed numerous candidate genes targeted by PLZF (McConnell *et al.*, 2003; Costoya *et al.*, 2004; Felicetti *et al.*, 2004). These target genes may have a great influence on the progression of melanoma, but their role in the aggressiveness of this cancer remains unknown.

For this reason, we used DNA microarray analysis to search for additional PLZF target genes. One of the most strongly regulated genes identified was pre-B-cell leukemia transcription factor 1 (Pbx1). Pbx1 is also a transcriptional regulator and a binding partner for a number of Hox proteins (Mann and Chan, 1996; Shanmugam *et al.*, 1997). We confirmed that Pbx1 is highly expressed in melanoma cells and that cell growth is markedly suppressed when its expression is knocked down. Furthermore, we identified HoxB7 as a binding

Correspondence: Dr S Higashiyama, Department of Biochemistry and Molecular Genetics, Ehime University Graduate School of Medicine, Shitsukawa, Toon, Ehime 791-0295, Japan.
E-mail: shigeki@m.ehime-u.ac.jp
Received 1 November 2005; revised 30 May 2006; accepted 31 May 2006; published online 24 July 2006

partner of Pbx1 in melanoma cells. We show here that PLZF suppresses the expression of Pbx1-HoxB7 target genes as well as Pbx1 itself and that dysregulation of this network owing to loss of PLZF may play an important role in the progression of melanoma.

Results

PLZF suppresses Pbx1 gene expression

Felicetti *et al.* (2004) reported that primary melanomas and melanoma cell lines completely lack PLZF gene expression and that enforced expression of PLZF in melanoma cell lines suppressed their growth *in vitro* and *in vivo*. We confirmed these results using 15 melanoma cell lines, including A375, 397 cell lines and their PLZF transfectants (data not shown).

We then examined which genes are repressed by PLZF in the melanoma cells by DNA microarray analysis. For these experiments, we constructed adenovirus vectors carrying the genes encoding PLZF and LacZ and used them to infect A375 and 397 cells at a multiplicity of infection (MOI) of 200. Several genes exhibited different levels of expression in PLZF-negative and PLZF-positive cells. We found that Pbx1 was the most prominently downregulated transcription factor in PLZF-positive cells (Table 1). Reverse transcription–polymerase chain reaction (RT–PCR) confirmed that Pbx1 mRNA expression in A375 cells was clearly and substantially reduced in a time-dependent manner after infection with the PLZF adenovirus (Figure 1a). The expression of Pbx1 mRNA decreased to 25% of that in LacZ-infected cells. In addition, the Pbx1 protein levels in the PLZF-infected cells decreased by approximately 40% when compared with cells infected with the LacZ adenovirus or non-infected cells (Figure 1b). We also obtained similar results in 397 cells.

Enforced expression of Pbx1 rescues growth suppression by PLZF

In order to determine the relative importance of PLZF-mediated downregulation of Pbx1 in the growth of melanoma cells, we examined the proliferation of stable PLZF-expressing melanoma cells transfected with the pME18S-Pbx1 or pME18S control vector. Pbx1 protein levels in the transfected cells were first estimated by Western blotting (Figure 2a). Pbx1 levels increased approximately 1.5- and 1.3-fold in A375P and A375 cells, respectively, in comparison with controls. We also examined transfection efficiency in these cells using the mixture of pME18S-Pbx1 and pME18S-ECFP (Enhanced Cyan Fluorescent Protein) vectors. We found that approximately 65% of the cells were CFP (Cyan Fluorescent Protein)-positive (Figure 2b, inset). We then investigated the growth of A375 and A375P cells after transient transfection with pME18S-Pbx1 or pME18S. Exogenous expression of Pbx1 did not cause further enhancement of A375 cell growth. This suggests that there was sufficient endogenous Pbx1 expression. A375P cells exhibited a marked downregulation of both endogenous Pbx1 expression and cell growth. This effect was partially (approximately 40%) rescued by the expression of exogenous Pbx1 (Figure 2b), thus suggesting the presence of a Pbx1-independent pathway in PLZF-transfected melanoma cells. We also obtained similar results in 397 and 397P cells (data not shown).

Table 1 Expression profile obtained by array hybridization

Genes[a]	*Description*	*Accession number*	*Ratio (PLF/LacZ)*	
tzfp	Testis zinc-finger protein	NM_014383	Up	> × 20
pnkp	Polynucleotide kinase 3′-phosphatase	NM_007254	Up	
mapk4	Mitogen-activated protein kinase 4	XM_008806	Up	
oas3	2′–5′ Oligoadenylate synthetase 3	NM_006187	Up	× 10– × 20
osmr	Oncostatin m receptor	NM_003999	Up	
fezl	Zygin I, isoform 1	NM 005103	Up	
tssc3	Tumor-suppressing subtransferable candidate 3	NM 003311	Up	
lmo6	Linn domain-only 6	NML006150	Up	
nfsl	Nfsl nitrogen fixation 1	NM_021100	Up	× 5– × 10
cir	Ebfl-interacting corepressor	NM_004882	Up	
btebl	Basic transcription element-binding protein 1	NM_001206	Up	
netl	P65 netl proto-oncogene protein	S82401	Down	< × 0.05
cacng7	Calcium channel gamma subunit 7	AF2S8387	Down	× 0.05– × 0.1
rgs6	Regulator of g-protein signalling 6	NM 004296	Down	
pbxl	Pre-B-cell leukemia transcription factor 1	NM_002585	Down	× 0.1– × 0.2
calbl	Calbindinl	NM_004929	Down	
arhgdig	rho gdp dissociation inhibitor gamma	NM_001176	Down	
chrna 10	Cholinergic receptor, alpha polypeptide 10	NM_020402	Down	
hgc6.2	Hgc6.2 protein	NM_014356	Down	
dc20	Dc20	AF311338	Down	
serpinhl	Serine proteinase inhibitor, clade h, member 1	NM_004353	Down	

Adenoviral transduction of PLZF was chosen for expressing PLZF in A375 and 397 cells instead of stably expressing of PLZF, because of (1) avoiding the bias of cell response for PLZF by cloning of drug-resistant cells and (2) controlling the expression level of PLZF. The levels of HoxB7, bFGF, Ang-2 and MMP9 were in the range of × 0.25– × 0.5. [a]These genes were common in both A375 and 397 cells in duplicate microarray analyses.

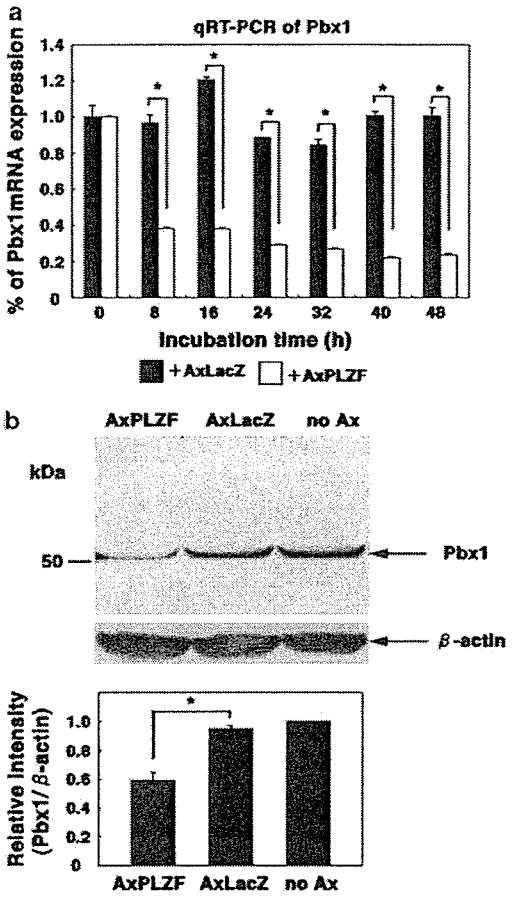

Figure 1 PLZF suppresses Pbx1 gene expression. (**a**) qRT–PCR of Pbx1 mRNA in A375 cells infected with LacZ or PLZF adenovirus. $*P<0.05$. (**b**) Upper panel: Western blot analysis of Pbx1 protein in A375 cells infected with LacZ or PLZF adenovirus and in uninfected cells. Lower panel: Relative intensity of Pbx1 proteins calculated as a ratio vs expression of β-actin. $*P<0.05$. AxLacZ, infection with LacZ adenovirus (MOI 200); AxPLZF, infection with PLZF adenovirus (MOI 200); no Ax, no infection. Each experiment was performed in duplicate.

PLZF physically interacts with the Pbx1 promoter

In order to demonstrate direct regulation of the Pbx1 gene by PLZF, we searched the Pbx1 promoter for a putative PLZF-binding site using the TFSEARCH program (Heinemeyer *et al*., 1998, http://mbs.cbrc.jp/research/db/TFSERCHJ.html), which suggested seven potential PLZF DNA recognition sequences located within a 3.0-kb region upstream of the transcription initiation site (Figure 3a). We then used a 3.0-kb fragment of the Pbx1 promoter in a reporter assay. The luciferase activity of Pbx1–3.0 was markedly suppressed in A375P, as compared to A375 cells (Figure 3b). Electrophoretic mobility shift assay (EMSA) was subsequently performed with nuclear extracts made from A375 cells infected with PLZF adenovirus and uninfected cells in order to identify the PLZF DNA recognition site in the Pbx1 promoter. Site 1 (2998 bp upstream) and Site 4 (2433 bp upstream) bound with factors in the A375 cell extracts without

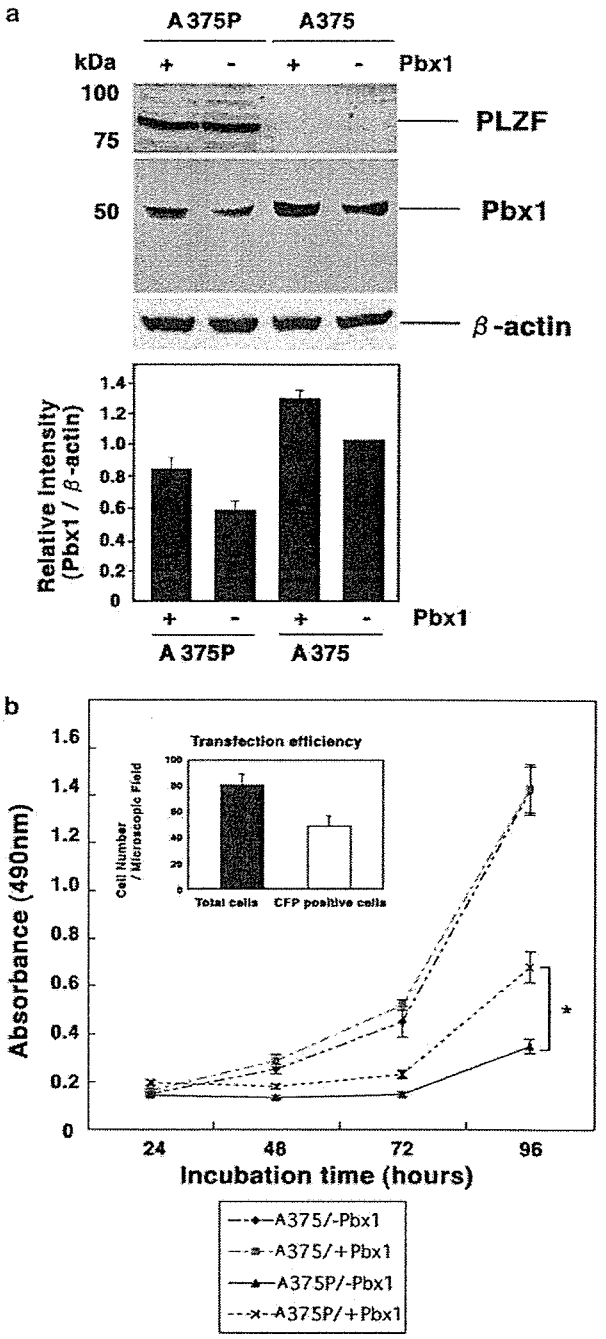

Figure 2 Enforced expression of Pbx1 rescues growth suppression of melanoma cells by PLZF. (**a**) Upper panel: Western blot analysis of PLZF and Pbx1 in A375 and A375P cells transfected with PME18S-Pbx1 or PME18S control vector. Lower panel: Relative intensity of Pbx1 protein, which was calculated as the ratio of Pbx1 vs β-actin. (**b**) Growth curves of A375 and A375P cells transfected with PME18S-Pbx1 and PME18S control vector. $*P<0.05$. Inset: Transfection efficiency of pME18S-Pbx1 was evaluated by counting CFP-positive cells transfected with both PME18S-Pbx1 and pME18S-ECFP.

PLZF expression (stars in lane 1 and lane 7), and formed another complex in the A375 cell extracts expressing PLZF (arrow in lane 2, Figure 3c). On the other hand,

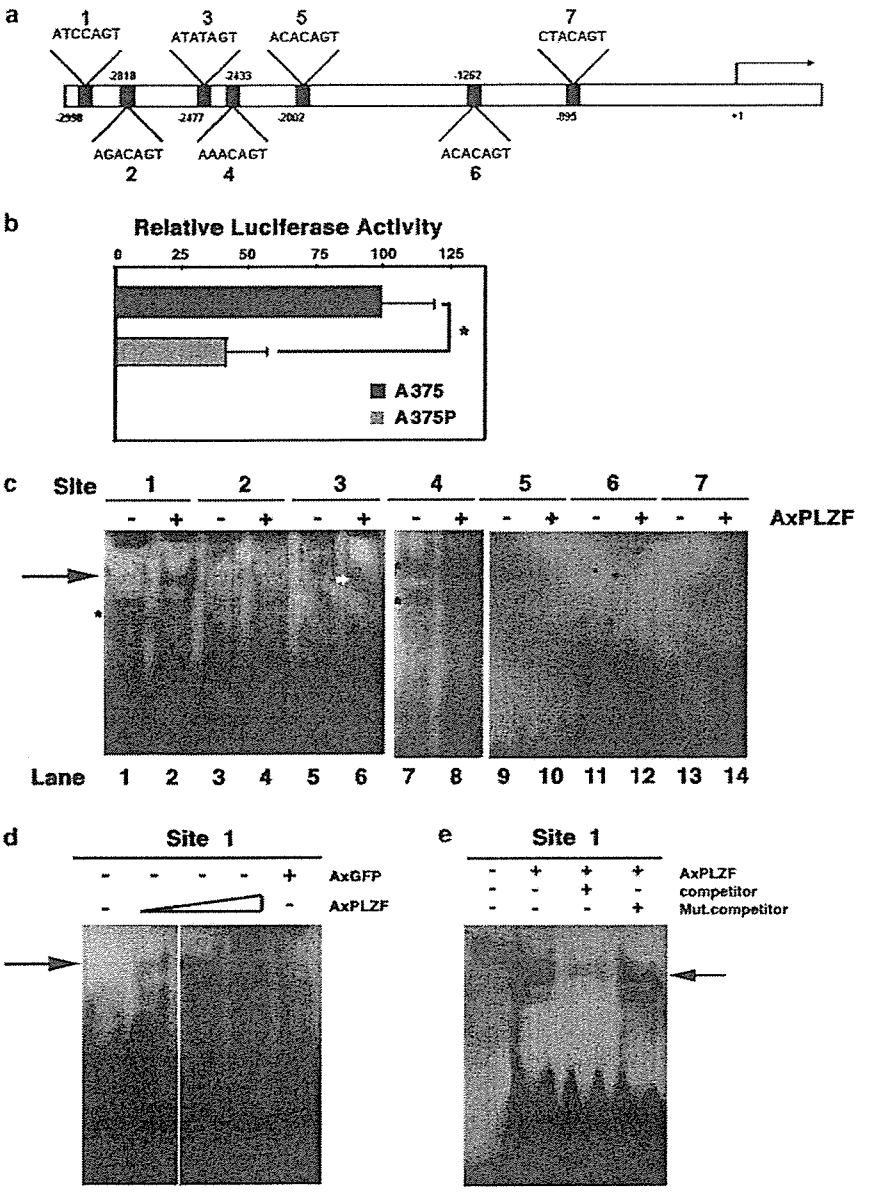

Figure 3 PLZF protein directly interacts with the Pbx1 promoter. (**a**) Schematic depiction of the Pbx1 promoter region and seven potential binding sites for PLZF (Sites 1–7). The +1 position corresponds to the initiation site of transcription. (**b**) Relative luciferase activity measured at 24 h after transfection of pGL Pbx1–3.0 into A375 cells and A375P cells. Each experiment was performed in triplicate and data represent the means±s.d. of three independent experiments. (**c**) EMSA carried out with nuclear extracts of A375 cells infected with PLZF adenovirus (MOI 100) and uninfected cells. White arrowhead in lane 6 shows stain. (**d**) Specificity of interaction between PLZF and Site 1 (an arrow) was confirmed by EMSA using nuclear extracts of A375 cells infected with PLZF (MOI 50, 100 and 200) or GFP adenovirus (MOI 200). (**e**) Interaction between PLZF and Site 1 (an arrow) was found to compete with unlabeled Site 1 but not with unlabeled mut. Site 1.

Sites 2, 3, 4, 5, 6 and 7 did not form additional complexes in the A375 cell extracts expressing PLZF, as compared to A375 cell extracts without PLZF (lanes 3–14, see comments on lane 6 in figure legends). To confirm the specificity of the interaction between Site 1 and PLZF, we carried out dose–response analysis and competition analysis. The interaction between Site 1 and PLZF exhibited a dose-dependent relationship (Figure 3d), and was completely abolished by the addition of the competitor (unlabeled Site 1). The competitor with the mutation (mutated Site 1, see 'Materials and methods') failed to abolish the PLZF–Site 1 interaction (Figure 3e). On the other hand, deletion of Site 1 from Pbx1–3.0 (Pbx1–3.0/ΔSite 1) did not show significant recovery of Pbx1 promoter activity (data not shown), indicating that Site 1 is an interactive site for PLZF, and is not sufficient for complete repression of Pbx1 gene expression. These results

suggest that repression of Pbx1 gene expression by PLZF is regulated by multiply direct and/or indirect mechanisms.

Melanoma cell growth is suppressed by Pbx1 small interfering RNAs

In order to further characterize the role of Pbx1 in melanoma cell growth, we examined the suppression of melanoma cell growth by Pbx1 knockdown using two types of small interfering RNA (siRNA) (siRNA1 and siRNA2). Mutated siRNAs (mut. siRNA1 and mut. siRNA2) were used as controls. We confirmed that transfection of A375 and 397 cells with Pbx1 siRNA1 significantly reduced Pbx1 mRNA (data not shown) and protein levels (Figure 4a). In addition, transfection of A375 and 397 cells with Pbx1 siRNA1, but not Pbx1 mut. siRNA1, caused marked and statistically significant suppression of cell growth (Figure 4b). These data suggest that Pbx1 is involved in cell growth of A375 and 397 cells. siRNA2 showed similar results as siRNA1 (data not shown).

Pbx1 binds HoxB7

Pbx1 forms complexes with a number of Hox proteins, and HoxB7 was expressed strongly in all melanoma cell lines tested (Care *et al*., 1996). We investigated whether Pbx1 interacts with HoxB7 in A375 and 397 cells. HoxB7 was immunoprecipitated from cell lysates and was then analysed by immunoblotting with anti-Pbx1 antibody. We detected a 52-kDa band corresponding to Pbx1 in both cell lines (Figure 5). We also found that an anti-Pbx1 antibody co-immunoprecipitated HoxB7 from the same cell lysates (data not shown).

Expression of HoxB7 target genes is downregulated by reduction of Pbx1

We investigated the effects of Pbx1 knockdown on the expression of HoxB7 and its target genes. Knockdown

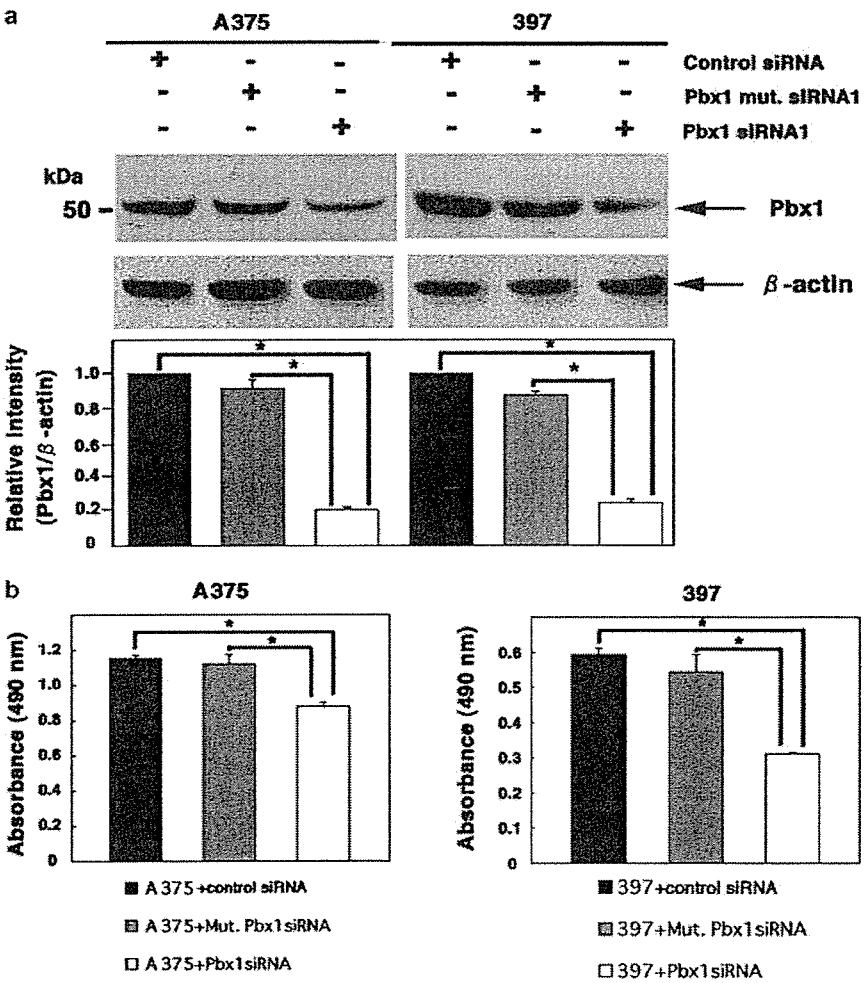

Figure 4 Melanoma cell growth is suppressed by Pbx1 siRNAs. (**a**) Upper panel: Western blot analysis of Pbx1 in control siRNA-, mutated-Pbx1 siRNA- and Pbx1 siRNA-transduced melanoma cells. Lower panel: Relative intensity of Pbx1 protein expression calculated as the ratio of Pbx1 vs β-actin. $*P<0.05$. (**b**) Cell proliferation of melanoma cells transfected with each siRNA. $*P<0.05$. Each experiment was performed in triplicate.